This manuscript is a preprint and has been submitted for publication in *Basin Research*. The manuscript has not undergone peer review. Subsequent versions of this manuscript may have different content. If accepted, the final peer-reviewed version of this manuscript will be available via the 'Peer-reviewed Publication' DOI link on the right-hand side of this webpage.

Please feel free to contact any of the authors directly to comment on the manuscript; we welcome feedback.

TURBIDITES, TOPOGRAPHY AND TECTONICS: EVOLUTION OF SUBMARINE CHANNEL-LOBE SYSTEMS IN THE SALT-INFLUENCED KWANZA BASIN, OFFSHORE ANGOLA

DANIELLE M. HOWLETT[1]*, ROB L. GAWTHORPE[1], ZHIYUAN GE[1], ATLE ROTEVATN[1] and CHRISTOPHER A. -L. JACKSON[2]

[1]*Department of Earth Science, University of Bergen, 5007 Bergen, Norway*

**E-mail: Danielle.Howlett@uib.no*

[2]*Basins Research Group (BRG), Department of Earth Science & Engineering, Imperial College, London SW7 2BP, U.K.*

KEYWORDS: Deep-water systems, sediment routing, seismic geomorphology, minibasins, salt tectonics, structural highs, tectono-stratigraphic evolution

ABSTRACT

Understanding the evolution of submarine channel-lobe systems on salt-influenced slopes is challenging as systems react to seemingly subtle changes in sea-floor topography. The impact of large blocking structures on individual deep-water systems is well documented, but understanding of the spatio-temporal evolution of regionally extensive channel-lobe systems in areas containing modest salt movement is relatively poor. We use 3-D seismic reflection data to map Late Miocene deep-water systems offshore Angola within a c. 450 ms TWTT thick interval. Advanced seismic attribute mapping tied to standard seismic stratigraphic, seismic facies analysis and time-thickness variations, reveals a wide variety and scale of alterations to sediment routing and geomorphology. Five seismic units (SU1-SU5) record a striking change in sediment pathways and structural relief within eight evolving minibasins. Observations within these units include gradual channel diversion through lateral migration during times of relatively high structural growth, opposed to abrupt channel movement via avulsion nodes during times of relatively high sediment accumulation. The results of the study led to the development of conceptual models for influences on deep-water systems during characteristic structural development in the contractional salt domain, these stages being initiation, maturity, and decay. The initiation stage contains small-segmented folds with mostly system bypass, while the maturity stage contains linked high-relief structures and prominent minibasins leading to ponding, large-scale diversion and localized slump deposits derived from nearby highs (SU1-SU3). The less studied final stage of topographic decay contains decreased length and relief of structures leading to

a more complicated array of channel-lobe bypass, diversion, ponding and subtle control on avulsion nodes (SU4-SU5). These observations contribute to the understanding of channel-lobe stacking, routing and control over transition zones in tectonically active areas, ultimately improving our general understanding of the effects of significant through to subtle sea-floor topography, and can be a guide in other salt-influenced basins.

INTRODUCTION

Sea-floor topography has a significant impact upon turbidity currents and their associated deposits. Structurally-controlled topographic sea-floor relief that influences deep-water gravity flows may be due to underlying normal faults (Haughton, 2000; Ge *et al.*, 2018; Mattos *et al.*, 2019; Muravchik *et al.*, 2019), thrusts with fault propagation folds (Clark & Cartwright, 2012; Tinterri *et al.*, 2017; Pinter *et al.*, 2018; Howlett *et al.*, 2019) or salt-cored structures (Mayall *et al.*, 2010; Hay, 2012; Oluboyo *et al.*, 2014). In addition, pre-existing sedimentary features may have an expression on the sea-floor, such as differential compaction of stacked channels (e.g. Ward *et al.*, 2017) and mass transport deposits (e.g. (Ortiz-Karpf *et al.*, 2015; Zhao *et al.*, 2019). Resulting structurally controlled sea-floor topography may result in turbidity current-fed systems being deflected, diverted, constricted or blocked (Kneller & McCaffrey, 1995; Prather *et al.*, 1998; Clark & Cartwright, 2009). Deep-water systems can be diverted for kilometres around large, high amplitude and long folds (Mayall *et al.*, 2010). Structural constriction occurs when deep-water systems are forced through a narrow spill-point between two structural highs, such as a segment boundary between two folds (Oluboyo *et al.*, 2014; Patacci *et al.*, 2015). Deep-water systems are blocked when confining topography traps the deep-water flows thereby creating a suspension cloud resulting in 'flow ponding' (Van Andel & Komar, 1969). Additional complicating factors include the angle of incidence with topography, internal flow parameters, such as grain size, density and stratification, as well as relative scaling between the height of the flow and the obstacle. These variable flow parameters influence fluid dynamics and resulting sediment deposition, and have been systematically modelled in flume tank experiments and numerical models (e.g. Kneller *et al.*, 1991; Kneller, 1995; Eggenhuisen & McCaffrey, 2012; Cartigny *et al.*, 2013; Aas *et al.*, 2014; Basani *et* *al.*, 2014; Howlett *et al.*, 2019). These concepts are applicable for individual flows but can also be extended to consider the accumulated effect of potentially thousands of these flows that build stratigraphic successions of the type and thickness observable in seismic reflections data. However, the behaviors of turbidite systems in structurally active regions can be very complex as both sea-floor topography and deep-water elements can vary spatially due to the active growth of intra-basinal structures, changes in sediment supply and routing. Consequently, understanding the detailed sedimentological response of extensive submarine channel-lobe systems with complex sea-floor topography, particularly in regions with mobile shale or salt substrates, remains challenging.

Regions with mobile salt substrate and deep-water systems include well-studied basins in the Gulf of Mexico (Smith, 2004; Prather *et al.*, 2012), eastern Mediterranean Levant Basin (Clark & Cartwright, 2009; Niyazia *et al.*, 2018), offshore Brazil, such as the Santos or Espirito Santo Basins (Gamboa & Alves, 2015; Rodriguez *et al.*, 2020), as well as along the west African margin, such as the Lower Congo or Kwanza Basins (Broucke *et al.*, 2004; Oluboyo *et al.*, 2014). Large-scale tectonic studies often utilize regional 2-D seismic data to understand structural development (Marton, 2000; Valle *et al.*, 2001; Tari *et al.*, 2003; Hudec & Jackson, 2004), and have developed useful methods to analyse stratal package geometries next to late stage diapir growth (Giles & Rowan, 2012; Rojo & Escalona, 2018). Tectono-stratigraphic studies often focus on the mature stages of structural growth, as this is when the influence of salt-cored structures, such as ponding and blocking, most drastically affects turbidite systems. Conversely, the impact during fold decay has often been underestimated. The intricate evolution of the deep-water systems depositing these stratal packages is observed in high-resolution 3-D seismic data through seismic attribute analysis. Most emphasis has been on the sedimentological response of individual channel-levee systems around solitary salt-cored structures (e.g. Gee & Gawthorpe, 2006; Gee *et al.*, 2007; Clark & Cartwright, 2009), with more recent study of the responses of lobe complexes to diapiric growth (Doughty-Jones *et al.*, 2017). Less attention has been devoted to the combination of these depositional elements (i.e. submarine channels, lobes) and on controls over the transitional zone from channel confinement to relative unconfinement, often referred to as channel-lobe transition zone (CLTZ) (Hofstra *et al.*, 2015; Brooks *et al.*, 2018), or locations for newly formed channel pathways referred to as avulsion nodes (Armitage *et al.*, 2012). The location of avulsion nodes is key for understanding exactly how channels move as structures grow and why some channels shift abruptly via these nodes while others gradually migrate laterally.

In this study we use an extensive 3-D seismic data volume to complete a detailed tectono-stratigraphic analysis within a series of minibasins in the Kwanza Basin, approximately 100 km offshore Angola. The stratigraphic interval-of-interest is within the Miocene and is composed of > 50 km long submarine channel-lobe systems trending both transversely and axially to structural strike. Our aim with this paper is to document the effect of salt-influenced sea-floor topographies on the routing and geomorphology of submarine channel-lobe systems. Specific objectives include (i) to understand the location and character of transition zones between depositional elements (i.e. CLTZ, avulsion nodes) in relation to sea-floor topography, and (ii) to develop an evolution model of channel-lobe systems that incorporates the mature growth and death stages of salt-cored folds. This work is novel as it explores the reasoning for abrupt channel movement via avulsion nodes versus gradual lateral channel migration, in response to dynamic underlying structures. Importantly, we present revised conceptual models of deep-water systems along evolving contractional salt domains, thereby providing a subsurface reservoir analogue for similar salt-withdrawal minibasins such as the stacked post-salt turbidite sandstones in Lower Congo Basin, offshore Angola (Huang & Zheng, 2019).

GEOLOGICAL SETTING AND STUDY AREA

The focus of this study, the northern Kwanza Basin, is bounded to the north by the Lower Congo Basin and to the south by the WNW-trending Cretaceous Kwanza seamounts (Figure 1a; Marton, 2000; Guiraud *et al.*, 2010). Similar to other sedimentary basins along the West African margin (offshore Gabon, Congo, Angola and Namibia), the Kwanza Basin formed during rifting and break-up of the Gondwana supercontinent in Late Jurassic to Early Cretaceous times (Brice *et al.*, 1982; Guiraud & Maurin, 1992; Karner & Driscoll, 1999; Moulin *et al.*, 2005; Jian-Ping *et al.*, 2008; Guiraud *et al.*, 2010).

The stratigraphy of the Kwanza Basin can be divided into pre-salt (Late Proterozoic-Barremian), salt (Aptian) and post salt mega-sequences (Albian-present). The pre-salt sequence is comprised mostly of continental deposits contained within intracratonic rift basins. A post-rift sag basin developed during the Barremian and restricted marine conditions leading to the deposition of a salt layer that was, on average, 3 km thick in the offshore Kwanza Basin (Hudec & Jackson, 2004). The initial deposits of the post-salt sequence (Albian) were predominately shallow water carbonates, followed by clastic progradation and deep-water sedimentation (Cenomanian-Eocene) (Anderson *et al.*, 2000; Lavier *et al.*, 2001; Valle *et al.*, 2001; Brownfield & Charpentier, 2006). Tectonic uplift and tilting of the margin ended marine conditions in the upslope, which resulted in shelf erosion with subsequent sediment delivery to downslope channel-lobe systems (Miocene-Oligocene) (Figure 2; Brice *et al.*, 1982; Anderson *et al.*, 2000; Jackson *et al.*, 2005). During the Pliocene through to present, low sediment influx and relatively high sea level were recorded in a sequence of condensed sections consisting dominatingly of hemipelagic clays and silts. There were limited channel-lobe systems during this time, largely constrained to river entry sites (Figure 2). Salt-related deformation preserved on the present-day sea-floor began shortly after the deposition of the Albian carbonates continuing until the present, with articulated periods of salt translation and increased salt growth (Figures 2-3; Duval *et al.*, 1992).

The structural style of the post-salt sequence is gravity-driven thin-skinned deformation creating up-dip extensional domain along the shelf and proximal slope, which is kinematically linked to a down-dip contractional domain (Marton, 2000; Valle *et al.*, 2001; Fort *et al.*, 2004; Brun & Fort, 2011; Quirk *et al.*, 2012). Within the extensional domain listric growth faults, grabens and rafts dominate, whereas the contractional domain contains mostly thrusts with fault-propagation folds, salt nappes, squeezed diapiric salt stocks and salt walls (Duval *et al.*, 1992; Lundin, 1992; Tari *et al.*, 2003; Guiraud *et al.*, 2010). We differentiate diapiric salt stocks and walls based on planform geometry in the study area, salt stocks (referred to as 'diapirs' in this study) contain more circular geometries rising from a point source (length:width < 3), while salt walls are substantially more elongated structures rising from a line source (length:width > 3) (Hudec & Jackson, 2007). Many contractional structures trend parallel to the shelf break due to gravitational gliding of the mobile substrate (Peel, 2014). The regional line from Hudec & Jackson (2004) suggests there are considerable basement steps in the Kwanza Basin, including directly east of the study area (Figure 1b). These blocks were uplifted around the Late Miocene (8 Ma) and likely influenced the ramp-syncline basin style of sedimentary fill observed within the older stratal packages of some minibasins in the study area (Pichel *et al.*, 2018).

DATA AND METHODOLOGY

The study utilises a time-migrated 3-D seismic reflection survey within the Kwanza Basin in water depths between 1800 m and 2300 m (Figures 1a). The study area is within the down-dip contractional salt domain, containing salt walls, diapirs and a thickened salt plateau (Figures 1b, 3). The eastern edge of the survey is approximately 30 km from the Late Miocene base of continental slope (Hudec & Jackson, 2004). The seismic survey covers an area approximately 3,500 km^2, with a 4-ms sample interval and a crossline and inline spacing of 12.5 and 25 m, respectively. The data is processed and displayed as zero phase, with a positive impedance contrast represented as a peak. No well calibration is available and stratigraphic age is based on correlation to regional lines (Hudec & Jackson, 2004) and nearby surveys (Oluboyo *et al.*, 2014). Data quality is generally good to excellent within the post-salt stratigraphy. The average frequency in the interval-of-interest is about 45 Hz, resulting in a maximum vertical resolution of 10 - 14 m assuming the vertical resolution is a quarter of the wavelength (Brown, 1999) and using an average seismic velocity between 1800 and 2500 ms^{-1}. The Miocene interval-of-interest is the shallowest and most readily imaged stratal interval with abundant submarine channel-lobe systems. The workflow for our study entailed: (i) defining a seismic stratigraphic framework and mapping bounding horizons, (ii) using time-thickness maps of the seismic units to constrain structural growth, subsidence and sedimentary system development, and (iii) utilizing a variety of seismic attribute maps and cross-sectional seismic facies to characterise the deep-water deposits and their evolution.

The seismic stratigraphic framework is based on identification of key seismic surfaces defined by stratal terminations, significant variations in seismic facies and time-thickness changes due to altering input directions of major sediment fairways (Figures 2, 4c; Table 1). Horizon stacks containing a number of surfaces for a defined interval are created within Paleoscan™ as preliminary inputs for the stratigraphic framework and are continuously edited due to the complicated isolating nature of the minibasins. Six horizons are used to define the interval-of-interest and these form the bounding surfaces of the main five seismic units (SU1-SU5) (Table 1).

Time-thickness variations within the seismic units are used as proxies for subsidence and uplift along the salt-cored structures, as well as to identify depositionally driven sediment accumulation along fairways (Figure 5). Thicknesses of beds along salt flanks were treated cautiously due to the reduced data quality in these areas. We have verified these stratigraphic thickness changes with cross-sectional geometries to validate lateral mapping of deep-water systems in the absence of well data. We have likely been conservative in widths of diapirs as wells have revealed salt bodies often extending beyond the confines of the 'chaotic' reflectors used for salt mapping (Jackson & Lewis, 2012; Jones & Davison, 2014). As the study is in the time domain, some geometric distortion is also expected along the salt flanks, but this has limited impact on the results of this deposition-based study.

Seismic attribute volumes, including spectral decomposition Red-Green-Blue (RGB) colour blends, are generated from the 3-D seismic volume and used to aid in mapping deep-water systems and seismic geomorphological-sedimentological analysis. The attribute spectral decomposition transforms data into the frequency domain, which results in a variety of frequency volumes (Othman *et al.*, 2016). In RGB colour blended maps, each colour corresponds to a specific frequency selected to image channel-lobe systems and slumps within the target interval. RGB colour blend maps do not simply display lithology changes but are also used to outline subtle bed thickness changes, structural edges and fluid varieties. Drastic variations in fluid (and gas) saturation within the Miocene deposits has the potential to boost amplitudes within sand-rich lobes and channels on attribute maps, thereby making the deposits more pronounced and visible than similar deposits in older, deeper stratigraphy (Maestrelli *et al.*, 2017). Although time windows around horizons can be defined for these attribute maps, the vertical resolution of these depends on the 'vertical smearing' during the frequency decomposition. For this study, the Constant Q method is used for frequency decomposition as quality of imaging representative of a seismic unit takes precedence over high vertical resolution (McArdle & Ackers, 2012). To aid in calibration and interpretation, the planform geometry and amplitude or frequency variations observed on attribute maps are accompanied by cross-sectional seismic facies analysis. Seismic facies represent the different elements of deep-water systems, such as submarine channels, lobes, slumps and slope deposits. These seismic facies are defined by reflection geometries and characteristics, such as amplitude, continuity and conformity (discussed in detail in *Seismic Facies and Depositional Environments*; Table 2).

PRESENT-DAY STRUCTURAL CONFIGURATION

The study area is comprised of 8 minibasins, up to 21 km long and 6 km wide, separated by a series of salt-cored highs (Figure 3). Most of the salt-cored highs can be observed on the modern sea-floor where they exhibit c. 85 to 450 ms TWTT of positive sea-floor relief. The planform length and cross-sectional geometry of these salt-cored highs distinctly vary spatially across the study area. Diapir geometry ranges from a relatively thin (c. 3 km diameter) basal pedestal with a drastically narrowing or vertically welded (secondary weld; sensu Jackson *et al.*, 2014) stock and piercing teardrop bulb (e.g. Diapir F; Figure 4a), to a pyramidal-shape with a wide (c. 7 km diameter) basal pedestal gradually narrowing upwards (e.g. Diapir Dii; Figure 4b). Salt wall geometries typically extend laterally over 30 km and are either piercing highs cutting stratigraphy over 2.5 s TWTT in height (e.g. Salt Walls A, B; Figure 4a) or subdued highs with concordant overlying stratigraphy (e.g. Salt Walls D, E; Figure 4a). Based on the spatial distribution, continuity and geometry of the salt-cored highs and corresponding minibasins, the structural style of the study area can be divided into two main domains: (i) an eastern domain defined by co-linear salt walls and elongated minibasins, and (ii) a western domain defined by variably orientated segmented and isolated salt walls, which gradually transition down-dip into a thickened salt plateau.

Eastern domain

The main structural elements in the eastern domain are four salt walls (Salt Walls A, B, C and D; Figures 3-4) and three intervening minibasins (MB1, MB2i, MB2ii and MB3; Figure 3). The minibasins are elongate NNW-trending (lengths c. 34 km, 5:1 length:width), with MB2ii being a southward extension of MB2i with a more circular planform geometry (length c. 18 km, 1.5:1 length:width). Deeper strata within some minibasins display a W-shape geometry due to the presence of salt pillows within the minibasin centres, whereas shallower strata have a U-shape geometry (e.g. between Salt Wall C and D; Figure 4a).

The elongate co-linear salt walls with apparent primary salt welds (below seismic resolution, < 50 m) separate salt withdrawal minibasins trending approximately parallel to the shelf break (e.g. between Salt Walls B, C and D; Figure 4a). The salt wall structural style transitions from Plio-Pleistocene piercing salt walls up-dip (e.g. Salt Walls A, B; Figure 4a) to subdued salt-cored highs with concordant overlying stratigraphy down-dip (Salt Walls C, D; Figure 4a). The sea-floor relief for the subdued salt-cored highs is relatively small (up to 110 ms TWTT) compared to the large relief (up to 450 ms TWTT) exhibited by the piercing salt-cored highs (Figure 3). The cross-sectional geometry of diapirs varies, generally appearing as detached salt bulbs with vertical, secondary weld (Diapirs Ci and Cii; Figure 4a) or occasionally a pyramidal shape with no vertical weld (Diapir Di; Figure 3).

Western domain

The main structural elements in the western domain are two salt walls (Salt Walls E, F; Figure 3) that gradually transition into a thickened salt plateau down-dip. There are four prominent minibasins in this domain (MB4, MB5, MB6 and MB7; Figure 3), with relatively circular planform geometries compared to the eastern domain (c. 21 km length, 2.4:1 length:width). Post-salt thicknesses are similar to the eastern domain (c. 2.4 s TWTT), but the Late Miocene eventually pinches out westwards onto the thickened salt plateau (Figure 4a).

The western domain contains more segmented and isolated salt-cored structures compared to the elongated co-linear salt walls in the eastern domain. Similar to the up-dip salt walls, Salt Wall E is NNW-trending. Salt Wall F contains a series of distinct segments exhibiting high topographic relief on the sea-floor with variable NE- and NW-trends (Fi, Fii and Fiii; Figure 3). The eastern edge of the thickened salt plateau trends NW, parallel to parental Salt Wall Fi (Figure 3). The salt plateau has a minimum areal extent of 1,230 km^2 (excluding the attached Diapir G), extending westwards beyond the study area. It is consistently thick (c. 1.25 s TWTT) with an undular top surface and small salt withdrawal minibasins (wavelength c. 1.6 km) (Figures 3, 4).

SEISMIC FACIES AND DEPOSITIONAL ELEMENTS

Comparison of the seismic facies with previous studies of deep-water systems aided in the identification of depositional elements and interpretation of sedimentary processes in the absence of well-based and lithological calibration within the study area (e.g. Abreu *et al.*, 2003; Deptuck *et al.*, 2003; Posamentier & Kolla, 2003; Janocko *et al.*, 2013; Oluboyo *et al.*, 2014; Hansen *et al.*, 2017). We define five dominant seismic facies based on integration of cross-sections and seismic attribute maps, referring to these as deep-water depositional elements as: (i) channels, (ii) levees, (iii) lobes, (iv) slumps, and (vi) slope deposits (Table 2).

Submarine channel

This seismic facies contains distinct defining characteristics, such as planform sinuosity and cross-sectional V- and U-shaped confinement of regularly stacked somewhat-chaotic high amplitude reflections (HARs) (Table 2). It is dominant spatially (extending lengths over 50 km) and temporally throughout the study interval. These V- and U-shaped deposits contain similar measurements for individual elements (c. 0.25 km wide and c. 20 ms TWTT thick), while dimensions for stacked complexes ranges from c. 0.25 km wide and c. 50 ms TWTT thick for V-shaped geometries, and c. 1 km wide and > 100 ms TWTT thick for U-shaped geometries. The base of these deposits may contain evident lateral accretion packages (LAPs), which appear as offlapping shingled reflections dipping towards the youngest deposit or a single continuous high amplitude reflection if the LAP is below seismic tuning thickness. Capping reflectors draping the U-shaped bodies may be ‘convex-up’ (positive-relief) or flat.

In planform, the V-shaped bodies tend to have lower sinuosities (near 1) relative to U-shaped bodies (greater than 1.5).

Similar seismic facies and seismic geomorphology have been observed in many other studies of deep-water depositional systems (e.g. Pirmez *et al.*, 1997; Prather *et al.*, 1998; Posamentier & Kolla, 2003; Hadler-Jacobsen *et al.*, 2005; Gee & Gawthorpe, 2006; Deptuck *et al.*, 2007; Janocko *et al.*, 2013; Oluboyo *et al.*, 2014; Hansen *et al.*, 2017; Niyazia *et al.*, 2018) and following these works, they are interpreted as submarine channel deposits. We will abide to the sedimentological terminology of channel belts and channel complexes, the latter referring to vertically stacked multi-story channel belts with varying offset (Collinson & Thompson, 1982). Channel complexes in this study are interpreted to contain both sand-rich and mud-rich channel fills based on cross-sectional geometry and amplitude contrasts on seismic attribute maps. High-amplitude sand-rich channel fills contain positive-relief due to differential compaction, whereas mud-rich channel fills contain flat capping reflectors if the channel form is thicker than 30 ms TWTT (Posamentier, 2003). Channel complexes are observed to be dominantly erosional, meandering and leveed. Erosionally-dominant systems are defined by lower sinuosities and V-shaped channel forms, while meandering systems contain higher sinuosities with LAPs and wide U-shaped channel forms. Leveed systems often contain U-shaped channel forms encased by high or low amplitude wedge-shaped geometries. Hybrids of these channel complex varieties are also common in the study area, such as wide meander belts encased by low amplitude levees or terraces.

Levees

In cross-section this seismic facies is characterised by two or more reflections that have a gull-wing-shape geometry and are located directly adjacent to submarine channels (Table 2). Reflections vary in amplitude, typically decreasing away from the channel axis before downlapping onto underlying deposits. This seismic facies is up to 80 ms TWTT height, and thins away from the channel axis over distances up to 12 km. These deposits are not always readily imaged on seismic attribute maps, especially when composed of dominantly low-amplitude reflections.

The geometry and reflection characteristics of this seismic facies has been recognised by other authors as external levees associated with channel complexes when the height of turbidity currents exceeds the confinement of the channel form (e.g. Posamentier & Kolla, 2003; Deptuck *et al.*, 2007; Janocko *et al.*, 2013; Oluboyo *et al.*, 2014). Often this overspill is fine-grained due to flow stripping, resulting in a mud-dominated deposit and potentially a low amplitude response in the seismic data (Table 2).

Lobes

This seismic facies is composed of distinctive, sub-parallel continuous high-amplitude reflection packages (HARPs) that are tabular to lobate in cross-section. It contains a maximum thickness of 50 ms TWTT, typically thinning and downlapping towards the outer edges (Table 2). On seismic attribute maps these deposits have a distinct tongue-shape down-dip of submarine channels. Individual lobe-shaped deposits generally contain a 'feathery' texture, distinguished by a branching outwards dendritic pattern. The boundaries of these lobes can be denoted by amplitude changes, such as a sudden dimming, although it can be difficult to differentiate lobes within the larger and thicker deposit. Lobes appear to prograde, backstep or compensationally stack one another in different minibasins (e.g. Figures 11, 14), with average lengths 4 - 5 km and widths 1 - 2 km. The larger deposit appears to reflect the shape of the minibasin accommodation it is infilling, with average lengths 8 - 18 km and widths 8 - 20 km.

These lobe-shaped deposits have been observed along the slope through to basin-floor, in both ponded and unconfined settings (Posamentier & Kolla, 2003; Gamberi & Rovere, 2011; Hay, 2012; Doughty-Jones *et al.*, 2017; McHargue *et al.*, 2020), and interpretations variably refer to these deposits as channelised lobes, frontal splays, sheet sands and submarine fans. We use the Prelat et al. (2010) hierarchical terminology and refer to the larger deposits as lobe complexes comprised of lobes with internal distributary channels forming dendritic patterns. Larger trunk channels feed these lobes and the dominant channel complexes sourcing this system are feeder channels (e.g. Figure 13). Taking into consideration tuning thickness effects on the seismic attribute maps, it is possible to differentiate the lobe axis and the outer lobe fringe based on amplitude contrasts due to the spatial variety of mud and sand distribution (e.g. Figures 9a, 13; Doughty-Jones *et al.*, 2017).

Slumps

This seismic facies consists of low-to-moderate amplitude reflections with a discontinuous and chaotic character forming bodies up to 50 ms TWTT thick and 15 km wide adjacent to salt-cored highs (Table 2). Internally these bodies may contain tilted reflections (internal thrusts) with strikes parallel to the edges of nearby topography. The base of these deposits is sharp and often truncates underlying reflections, whereas the top surface is generally irregular and undulatory. On seismic attribute maps these deposits can blend in with surrounding mud-rich background slope deposits but appear speckled.

The distinctly chaotic seismic facies is interpreted as a gravity-driven mass-wasting process, such as mass transport complexes, debris flows and slumps (Posamentier & Kolla, 2003; Olafiranye *et al.*, 2013; Ortiz-Karpf *et al.*, 2015; Doughty-Jones *et al.*, 2019; Wu *et al.*, 2020). Such mass wasting processes can be erosive when frictionally attached, thereby scouring the underlying strata on a seismic-scale (Bull *et al.*, 2009). Due to the location of these deposits adjacent to salt-cored structures and presence of syn-depositional thrusts, we interpret most of these deposits as slumps locally sourced off the flanks of topographic highs (Martinez *et al.*, 2005). The speckled appearance observed on seismic attribute maps may be due to these internal thrusts or megaclasts incorporated in the deposit (Ortiz-Karpf *et al.*, 2017).

Slope deposits

The characteristic signature of this seismic facies is the low to moderate amplitude reflections, which are parallel and conformable to underlying deposits (Table 2). These deposits range from a few reflections up to hundred's of ms TWTT, continuing across the minibasins laterally for ten's of kilometers. On seismic attribute maps this seismic facies is characteristically low amplitude and dark, allowing a distinctive interpretation of the other facies and geomorphologies.

Similar seismic facies have been observed in many areas, believed to be the deposition of pelagic and hemipelagic mud and silt during sediment starvation in low-energy environments (Hadler-Jacobsen *et al.*, 2007; Oluboyo *et al.*, 2014). It should also be noted that not all of these deposits are from suspension settling and some of these sheet-like deposits may be fined-grained, low-density turbidity currents (Straub & Mohrig, 2009).

TECTONO-STRATIGRAPHIC EVOLUTION

The seismic-stratigraphic framework for the study interval is based on six key seismic horizons that sub-divide the Miocene interval-of-interest into five seismic units (Table 1). The following sections will describe time-thickness variations (Figure 5) and outline the main sediment pathways on representative seismic attribute maps for each unit (Figures 6, 7, 9, 11, 14).

Seismic Unit 1 (SU1)

SU1 is the oldest seismic unit in the study and is dominated by hemipelagic deposits contained within the up-dip minibasins (MB1, MB2i, MB2ii, MB3 and MB4) by salt walls (Figure 6). SU1 thickness is relatively constant at c. 40 ms TWTT throughout the majority of the minibasins. Subtle thicks occur at the sediment entry points in MB2ii, the southern portion of MB1 and in the centres of MB2i and MB3 (c. 60 ms TWTT; Figure 5a). SU1 is thinnest in MB4 where the unit spills from the up-dip MB3 through a segment boundary along Salt Wall D (Figure 6).

Based on the volume windows provided by a series of attribute maps, SU1 is comprised primarily of 36% hemipelagic deposits, 34% poorly imaged lobes and 30% channel complexes. The channel complexes can be further classified as 53% lacking observable LAPs and 47% containing LAPs. Some of the lobe deposits are difficult-to-resolve on the seismic attribute maps and are inferred where trunk channels branch outwards before terminating. This unit is comprised of sediment Pathways A and B, which both enter the study area at an orientation transverse-to-structure (Figure 6). The northern Pathway A consists of multiple sinuous channel complexes that are strongly influenced by salt-cored structures within the study area, while the southern Pathway B is composed of lobes confined within MB2ii.

Pathway A

The channel complexes within Pathway A enter MB1 transversely to the structural trend, between Salt Wall A and Diapir A (Figure 6). The northern channel complex (A_N) contains low sinuosity (ave. 1.06) channels diverted northwards to trend parallel along Salt Wall B, while the main high sinuosity (ave. 1.64) channel complex crosses the south end of Salt Wall B into MB2i and is funnelled between Diapirs Ci and Cii into MB3. Older channel complexes are diverted north of these diapirs and across Salt Wall C, where the system deposits a series of lobes with dimensions c. 4 km by 2 km in MB3 (Figure 6). The sinuosity of Pathway A_N channels increases in MB3 (from ave. 1.05 to 1.79) as they are diverted northwest towards a segment boundary along Salt Wall D. Once the channel complex crosses into MB4, the meander belt wavelength increases drastically (from c. 2.5 to 10.8 km) and the system is diverted north along the salt walls before exiting the study area.

The most southern channel complex within Pathway A (A_S) enters MB2ii as a series of channel complexes without evident LAPs. One channel complex feds small lobes (ave. 1.4 km by 2.6 km) to the south of the channel axis before terminating as larger lobes (ave. 2.0 km by 5.0 km) blocked by down-dip Diapir D.

Pathway B

Pathway B lies to the south of Pathway A, in the southeast of the study area and consists of a large lobe complex (c. 6.5 km by 11.8 km) entering transverse to structural strike, south of Diapir A (Figure 6). Individual lobes are inferred by subtle changes in distributary channel orientation (c. 12.5 m wide), and although some distributary channels are diverted north along Salt Wall D, the lobe complex is largely blocked by Diapir D and confined within MB2ii.

Seismic Unit 2 (SU2)

SU2 is more laterally extensive than SU1, extending into distal down-dip minibasins, as well as having different sediment input directions and locations (Figure 7). The isochron thicks for SU2 are pronounced along the main sediment pathway up to 200 ms TWTT, most notably within MB2ii (Figure 5b). Additional isochron thicks are within MB4 and MB6 (c. 130 ms TWTT), before thinning down-dip into MB5 and MB7 (c. 45 ms TWTT).

The seismic facies for this seismic unit is 47% dominated by extensive channel complexes, with 37% hemipelagic deposits and 15% lobes comprising of the rest of the unit. The channel complexes can be sub-divided into 51% lacking observable LAPs and 49% containing LAPs. As with SU1, the lobes are difficult to resolve and often inferred by the termination of feeder channels that are observed with an outward branching pattern. The main sediment routing system for SU2 is Pathway C, channel complex entering from the southeast corner of the study area.

Pathway C

Pathway C is orientated oblique-to-structure and consists mainly of channel complexes trending broadly northwest (Figure 7). There is one main c. 2.5 km wide and c. 80 ms TWTT thick channel complex with LAPs (Figure 8). Sinuosity is highest for the oldest LAPs within MB2ii (ave. 2.77) and decreases significantly (ave. 1.08) in the youngest LAPs within MB2ii and MB6. The northwards diverted channels continue around the salt-cored relief of Diapirs Ci and Cii until the channel width decreases to near seismic resolution and thin lobes may be deposited.

There is potentially a series of avulsion nodes overtop of Salt Wall D, along the outer meander bends of main channel belts (Figure 8a, b). These nodes fed smaller channel complexes both northwards into MB3 and westwards into MB6 towards MB7. Instead of minor avulsion nodes these could also simply be channels cross cutting, as it is not possible to fully distinguish the channel boundaries at the seismic resolution. On the western side of MB6 the channel complexes encounter a narrow c. 5 km long ‘chokepoint’ between Salt Wall Fi and Diapir G, where they coalesce into an erosional channel complex that feeds thin axial lobes (c. 30 ms TWTT) within MB7.

The main channel complex with LAPs continues towards the northwest, initially containing high sinuosity channels (ave. 2.12) as it is apparently funnelled between Salt Wall Fiii and Diapir F before spilling into MB4 (Figure 8c). As the main channel complex passes from MB4 into down-dip MB5, the sinuosity decreases (ave. 1.10) along the steeper gradient near Diapir E, but increases once again (ave. 1.63) further into MB5 where the channel meanders are translating down-flow in a lower gradient area in the minibasin centre (Figure 8d). The channel complex contains no levees alongside Salt Wall Fi and decreases in sinuosity before exiting the study area as an axial system (Figure 8e).

Seismic Unit 3 (SU3)

SU3 has different sediment input locations and directions than SU2, thereby shifting the unit thicks from the south of the study area to the north (Figures 5c, 9). The isochron thicks for SU3 are dominated by the relatively older sediment Pathway D in the northeast, largely within MB2i (c. 180 ms TWTT; Figure 5c). Relative thicks up to 85 ms TWTT are within the down-dip minibasin centres for younger sediment Pathways A and B. Unlike SU2, deposition for SU3 does not continue into MB7.

SU3 is comprised of 39% lobes, 31% hemipelagic deposits, 26% channel systems and 5% slumps. The channel complexes can be further sub-divided into 65% containing LAPs and 35% lacking observable LAPs, while the lobes can be sub-divided into 64% highly channelised lobe complexes and 36% difficult-to-resolve lobes. SU3 can be divided into a lower (older) sub-unit dominated by lobe complexes with low sinuosity trunk channels from Pathway D and an upper (younger) sub-unit consisting of widespread, high sinuosity, initially transverse-to-structure channel-lobe systems within sediment Pathways A and B (Figure 9).

Pathway D

The older sub-unit of SU3, Pathway D, is a substantial (c. 185 km^2 area) sediment routing system and the only system to enter from the northeast (Figure 9). Pathway D is composed of numerous lobe complexes which can be sub-divided into three phases based on reflection characteristics and channelisation (Lobes Di, Dii and Diii; Figure 10a). The oldest lobe complex (Di) is composed of parallel low to medium amplitude reflections with a few notable down-laps indicating lobe fringes. While there are only a few observable channels, the extensive lobes are largely confined within MB2i with some spill-over across Salt Wall C into MB3 (Figure 10a). Lobes within Dii are comprised of medium to high amplitude reflections with numerous low sinuosity (ave. 1.07), c. 300 m wide trunk channels, which are diverted around Lobe Di topography and deposit lobes further down-flow within MB2i and MB3. The youngest lobes (Diii) contain high amplitude continuous reflections with indistinguishable lobe fringes. These lobes have few trunk channels (c. 200 m wide) but contain numerous distributary channels (c. 20 m wide).

Pathway A

The upper (younger) section of SU3, sediment Pathways A and B, return to a transverse-to-structure orientation of sediment routing. Pathway A is composed of a series of main channel complexes along a c. 9 km transect, similar to Pathway A in SU1 except here there are a greater number of thicker channel complexes (Figure 9). This sediment pathway splits into a NW-trending pathway (A_N) and a westward-trending pathway (A_S) (Figure 9). The low sinuosity channels of A_N (ave. 1.12) are diverted west of Pathway D and over Salt Wall C down-dip into MB3. As the channels cross over Salt Wall D, they either decrease in width to below seismic resolution or they deposit thin, low-amplitude, axial lobes in MB4 (Figure 9). Pathway A_S continues transverse-to-structure, confined between Diapirs Ci and Cii, continuing towards Salt Wall D. The main channel complex is funnelled between Salt Wall Fiii and Diapir F, although some minor channels deposit a series of lobes south of Salt Wall Fiii (Figure 9). The channel complex entering MB5 is confined between the southern end of Diapir E and a c. 18 km^2 detached slump derived off the flank of the nearby diapir (Figure 10b, c). The channel complex decreases sinuosity (ave. 1.67 to 1.02) and width (c. 1.5 km to 0.5 km) across this corridor and continues axially along MB5 and northward out of the study area (Figure 10b). A small-avulsed channel is intricately routed through the tortuous slump topography (Figure 10b).

Pathway B

Pathway B appears similar in extent and geomorphology to the blocked lobe complex within Pathway B of SU1. Pathway B also consists of transverse-to-structure input south of Diapir A, depositing feathery texture lobes up-dip of Diapir Dii (Figure 9). In addition, the lobes appear to be cut by a younger channel complex continuing westwards with accompanying unconfined overspill deposits.

Seismic Unit 4 (SU4)

SU4 is more extensive than SU3 as it continues into the down-dip MB7 and is dominated by widespread channel-levee systems (Figure 11). The time-thickness map for SU4 thicks largely follow the main sediment pathways through the centre of the study area up to c. 150 ms TWTT near Salt Wall B (Figure 5d). Relative thicks of c. 70 ms TWTT follow stacked channel complexes that continue northwest into MB5 or southwest into MB7, terminating as lobes before spilling into an adjacent c. 16 km^2 minibasin.

SU4 is predominantly composed of 50% channel systems and 41% lobes, with minor 9% hemipelagic deposits. The channel complexes dominating the northern section of the study area can be sub-divided into 56% containing LAPs, 32% lacking LAPS and 12% large stacked systems. Three main sediment fairways occur within SU4, Pathways A, B and E, enter the eastern side of the study area at a high angle to structural strike. The main sediment pathway is the central Pathway A, which consists of numerous major channel complexes extending down-dip into MB5 and MB7. Pathway B is a lobe complex largely confined to MB2ii, while Pathway E comprises of numerous relatively small channel complexes.

Pathway A

Pathway A is an extensive sediment fairway and enters MB1 as a series of channel complexes along a c. 5 km wide section across Salt Wall A and continues down-dip into MB2ii, MB6 and MB7 (Figure 11). This pathway can be divided into a northern channel complex (A_N), a central collection of channel complexes (A_C), and a far-reaching > 43 km long southern channel complex (A_S). Collectively, the channel complexes have high sinuosities and meander belt widths within MB1 (ave. 2.58 and 1.7 km, respectively) which substantially decrease down-dip of Salt Wall B (Figure 11).

The southern channel complex of Pathway A (A_S, Figure 11) firstly deposits a lobe complex (Ai) extending southwest into MB2ii, which is later eroded by an extensive low sinuosity channel complex. This channel complex is diverted c. 1.6 km south around Diapir Cii and contains locally well-developed levees, particularly on the southern side of the channel complex. Channel sinuosity increases immediately down-dip of Salt Wall C (ave. 1.2 to 1.40) and feds a series of backstepping lobes (Aii and Aiii) within MB6 (Figure 11). The main channel complex continues west, diverted c. 3 km south by Salt Wall Fiii, and continues as a narrow, erosive channel through the confining 'chokepoint' between Salt Wall Fi and Diapir G (Figure 12a-c). Upon entering MB7 the channel complex becomes unconfined through the CLTZ (Figure 12d) and deposits a widespread down-dip terminal lobe complex (Aiv) up to 100 ms TWTT thick (Figure 12e). The trunk channels of the lobes are c. 0.3 km wide, while the distributary channels are at the limit of seismic resolution and appear as a feathery texture on RGB attribute maps.

The central channel complex of Pathway A (A_C, Figure 11) crosses Salt Wall B and subsequently decreases in average sinuosity (ave. 3.20 to 1.46) and meander belt width (ave. 2.5 km to 1.3 km). Within MB3 and MB4 these channels are high sinuosity (ave. 2.1), but the youngest channel belt sinuosity decreases (ave. 1.1) along Diapir F. The system deposits a series of lobes along the confining Salt Wall Fi and leaves the study area as axially-trending channel complexes.

The northern channel complex of Pathway A (A_N) is the first stacked channel complex, containing a complex width of c. 1.2 km, relatively high sinuosities (ave. 1.5 in MB3) and a total thickness up to 85 ms TWTT (Figure 11). The channel complex is diverted axially along MB4, with decreasing sinuosity (ave. 1.5 to 1.2) and a lack of LAPs. An older channel complex along this sediment pathway crosses Salt Wall D before being diverted north into accommodation down-dip of Salt Wall D (Figure 13). The channel complex continues to trend axially along the centre of MB4 (Figure 13). Sinuosity and meander belt width initially increase into the accommodation (ave. 1.06 to 1.55 and 0.7 km to 1.5 km, respectively) before finally decreasing along the salt walls (ave. 1.16 and 1.1 km, respectively).

Pathway B

Pathway B is essentially a continuation of the minor sediment Pathway B from SU3 but contains more defined lobes and a younger high sinuosity (ave. 1.59) channel complex eroded by Pathway A_S (Figure 11). The lobes once again fill the accommodation within MB2ii and are blocked to the southwest by Diapir Dii.

Pathway E

Due to down-cutting from a younger channel complex in SU5, it is not possible to document the exact entry point for Pathway E and there may be a single entry point or multiple entry points along a c. 5 km transect (Figure 11). Pathway E contains numerous channels crossing MB2i at a high angle to structures with few observable LAPs, low sinuosities (ave. 1.07) and a narrow channel width of c. 0.15 km.

Seismic Unit 5 (SU5)

SU5 is defined by a dominance of large stacked channel complexes and terminal lobes within the northern section of the study area (Figure 14). Relative isochron thicks on the time-thickness map are largely contained along a pathway continuing through MB1, MB2i, MB3 and MB4, ranging from 120 to 150 ms TWTT (Figure 5e). The unit gradually thins towards the south as the channel levees down-lap onto SU4. There is no indication of thinning of SU5 across the salt walls, apart from subtle thinning over Salt Wall E.

The boundary between SU4 and SU5 is marked by a notable change in seismic facies. While SU4 is dominated by solitary channel complexes, SU5 is composed of thickly stacked or erosional channel complexes and laterally extensive lobes. Overall SU5 comprises of 44% channel systems, 42% unconfined lobes, and 14% hemipelagic deposits. Channel complexes can be further sub-divided into 40% large stacked complexes, 40% large erosional complexes with terraces and 20% smaller complexes with or without observable LAPs. There is one main transverse-to-structure sediment fairway for SU5, Pathway E, composed of channel complexes and a lobe complex.

Pathway E

Pathway E is comprised of three dominant channel complexes with LAPs and one terminal lobe complex (Figure 14). A series of major avulsion nodes on the channel-levee systems are located along the structural highs of Salt Walls B, C, D and E, situated on the outer bends of the channels (Figure 14). Avulsed channels preferentially divert northwards as axial systems. Two of the channel complexes (E_i and E_{iii}) contain high-amplitude stacked channels with c. 100 ms TWTT thicknesses and c. 1.5 km channel complex widths, containing low to medium amplitude levees > 2 km. The third channel complex (E_{iv}) is erosional with c. 120 ms TWTT thickness and c. 1.3 km channel complex width, encased by low amplitude flat-topped terraces. Overall, Pathway E can be sub-divided into four distinct sediment pathways (E_i, E_{ii}, E_{iii} and E_{iv}) based on relative age (oldest to youngest) and routing.

The oldest channel complex of Pathway E (E_i, Figure 14) is the continuation of a large stacked channel complex from SU4 (A_N; Figure 11) with LAPs and an average channel complex width c. 1.2 km within MB3 (Figure 15a). This system crosses Salt Wall D and diverts northwards into an axial system, with meander belt width and sinuosity gradually decreasing (ave. 2.0 to 1.4 km and 1.5 to 1.3, respectively) before leaving the study area (Figure 14).

Channelised lobes are the dominant component of Pathway E within MB5 and the southern portion of MB4 (E_{ii}; Figure 14), with Pathway E_i acting as the main feeder channel. A major CLTZ for the system occurs immediately down-dip of Salt Wall D, depositing a series of terminal lobes. Lobe geometry generally reflects the shape of the minibasin, with average dimensions of 5.4 km length by 1.8 km width in MB5 and 7.6 km length by 1.6 km width in the southern section of MB4. Lobe stacking patterns vary spatially throughout the minibasins, backstepping in the southern reaches of MB4, prograding over the southern tip of Salt Wall E, and mostly compensationally stacking within MB5 (Figure 14). The feathery-textured distributary channels within the lobes show diversion along Salt Wall Fi (Figure 14). Lobes along this pathway are also deposited to the south of the main channel complex within MB3 and MB4 (ave. 6.6 km length by 2.9 km width), from minor avulsion nodes (Figures 14, 15a).

The second youngest main channel complex of Pathway E stems from an avulsion node above Salt Wall C (E_{iii}; Figure 14). The wide channel meander belt width reduces after crossing Salt Wall C (3.1 km to 1.5 km) until the channel complex reaches Salt Wall D. Here, it largely follows the structure for 17 km before diverting westwards and exiting the study area.

The youngest channel complex of Pathway E largely infills MB2i (E_{iv}; Figure 14) and has a remarkably different geomorphology from the older channel-levee systems in SU5 (E_{i}-E_{iii}), as E_{iv} channels have high sinuosities (ave. 2.49) and meander belt widths (ave. 3.0 km) (Figures 14, 15b). The individual erosional channel belts contain an average width of 250 m and height of 40 ms TWTT, forming an extensive down-cutting channel complex > 100 ms TWTT thick, surrounded by low amplitude terraces (Figure 15b).

DISCUSSION

Summary of results

The five seismic units essentially record a diminishing impact of structural topography with time within a c. 450 ms TWTT Late Miocene interval (Figure 16). Early transverse-to-structure channel-lobe systems within SU1 are diverted axially northwards but are mostly contained to up-dip minibasins by high-relief salt-cored structures. Obliquely-trending sediment input from the southeast within SU2 is more laterally extensive across all of the minibasins with less obvious structural influence, although sediment pathways within SU2 are diverted northwards into axial systems before exiting the study area (Figure 16a). The drastic change in sediment input locations between SU1 and SU2 is likely due to salt movement up-dip blocking and diverting the sediment routing systems. Sediment input changes again between SU2 and SU3, with SU3 containing major obliquely-fed systems from the northeast and minor transversely-fed systems from the east (Figure 16b). Unit depocentres subtly shift from the south of the study area towards the north and there is a substantial seismic facies evolution from relatively narrow channel complexes to a dominance of massive lobe complexes (Figure 5b, c). This is likely due to a combined salt movement re-directing major sediment routing systems outside the study area, and increased subsidence in the northeast allowing the deposition of large lobe complexes rather than bypassing channels. Transverse sediment input becomes more prominent during SU4 and the sediment pathways are, once again, more extensive across all minibasins due to the dominating regional depositional gradient (Figure 16c).

Although the initial sediment input direction remains transverse-to-structure between SU4 and SU5, there is a major change in channel geomorphology from relatively narrow and thin low sinuosity channel complexes towards wider, thicker high sinuosity stacked channel complexes. The main pathway in SU5 contains three major avulsion nodes from where systems are directed northwards as channels complexes or westwards as lobe complexes (Figure 16d). The youngest channel complex in SU5 uniquely contains highly erosive channels bound by low amplitude, likely mud-rich terraces, and have high sinuosity and wide meander belts. The terraces are likely to have either formed through entrenchment or point bar accretion processes (Hansen *et al.*, 2017). While entrenchment can occur through vertical incision or punctuated channel migration (Maier *et al.*, 2012), point bar accretion is the progressive widening of channel bends within the LAPs. These channels and associated terraces are comparable to those observed by Deptuck et al. (2007), who described this phenomenon through the plug-and-cut mechanism with erosion on the outer-bend leading to increased channel sinuosity.

The regional dip for the study area is generally towards the west (Figure 3), but there is a pattern of northward diversion of deep-water systems through the seismic units. SU1 and SU2 both display significant diversion of initially transverse channel complexes into northward-trending axial systems along the salt walls (Figure 16a, b). The youngest unit SU5 is restricted within the northern section of the study area and the major stacked channel complexes show a pattern of northward directed avulsion (Figure 16d). From a sedimentological perspective, the SU5 channel complexes can be interpreted as a compensational infill of accommodation adjacent to SU4 systems (Figure 16d). From a structural point-of-view, it is also possible to have a subtle structural north-dipping gradient from a combination of re-activated tilted fault blocks and corresponding salt movement due to Neogene basement uplift along the shelf and upper slope (Hudec & Jackson, 2002; Hudec & Jackson, 2004). The structural gradient may also be created through the local build-up and continued topographic relief of the salt plateau in the southwest of the study area. Salt translation towards the southwest is evident near Salt Wall F, where systems initially continued through a topographic low between Salt Wall Fiii and Diapir F (Figures 7, 9) but later continue over Diapir F (Figures 11, 14) likely due to amplified topographic relief on Salt Wall Fiii associated with slower salt translation near the salt plateau.

Structural Growth versus Sediment Accumulation Rate

From a tectono-stratigraphic perspective, the sediment record in a tectonically active basin is the interaction between structural growth and sediment accumulation rate (e.g. Broucke et al., 2004). For example, in rift basins, different combinations of structural grow rate (rift initiation vs rift climax) and sedimentation rate (overfill vs starved) result in different syn-tectonic stratigraphic patterns (Gawthorpe et al., 2004; Ravnås & Steel, 1998; Gawthorpe & Leeder, 2000). However, the complex nature of deep-water systems and salt tectonics make such synthesis more difficult to achieve. Based on examples from this study and literature, we propose that the influence of salt-cored structures on the location and geomorphology of deep-water systems can be viewed in terms of the ratio between the rate of salt structure growth and the rate of sediment accumulation (Figure 17). We define the rate of structural growth as the salt-cored relief above salt walls compared to minibasin subsidence. On the other hand, the rate of sediment accumulation is a relative indication of incoming sediment pathways, even though in reality it is a complexity controlled by external factors outside of the study area such as climate. Similar relationships between the relative rates of sediment delivery and subsidence have been explored in terrestrial minibasins (Banham & Mountney, 2013).

Periods of dominantly high relative rates of structural growth relative to sediment accumulation (left side of Figure 17) have been widely documented to result in blocking and ponding or large-scale diversion on turbidite systems (e.g. Gee & Gawthorpe, 2006; Clark & Cartwright, 2009; Clark & Cartwright, 2012). Large-scale diversion of channel complexes distances greater than 5 km along structural relief (e.g. SU1 Pathway A; Figure 17a) is often accompanied by a decrease in average meander belt width and sinuosity. Sometimes this major diversion can be towards segment boundaries, observed as < 2 km long topographic lows between two folds (Figure 17b), and this has also been seen in the salt-walled minibasins of the Lower Congo Basin (Oluboyo *et al.*, 2014). The large-relief folds can also create substantial accommodation down-dip due to associated salt withdrawal and subsidence, leading to gradual channel diversion towards this topographic low and an increase in average meander belt width (Figures 13, 17d). Segment boundaries also lead to a narrowing of the sediment fairway and with channel complexes being more erosional. Down-flow of the segment boundaries channels often widen and increase in sinuosity in the down-dip minibasin (e.g. SU4 Pathway A_S; Figure 17c). Chokepoints, observed as > 2 km elongated narrow passageways between two topographic highs, can also be a major control on the location of where confined flows become unconfined, otherwise known as the channel-lobe transition (CLTZ) (e.g. SU4 Pathway A_S; Figures 11, 17e). If the unconfined flows encounter blocking high relief salt-cored structures, lobe complexes will deposit in the up-dip areas and likely completely infill the accommodation space (e.g. SU4 Lobe Aiv; Figure 17f). When the angle of incidence between the unconfined flow and strike of the structure is oblique, the lobe complex and internal distributary channels will be elongated and diverted axially, parallel to the structural strike (e.g. SU5 Pathway E_{ii} and SU1 Pathway B; Figure 17g).

In contrast to situations when structural growth rate outpaces sediment accumulation, times of high rates of sediment accumulation relative to structural growth (right side of Figure 17) have also been commonly observed within intra-slope deep-water systems (e.g. Jobe *et al.*, 2015). Channel complexes may be diverted small distances (< 5 km) around structural relief, and sinuosity may decrease slightly along the strike of the structure but increase again immediately down-dip to long-profile gradient changes (e.g. SU4 Pathway A near Diapir Cii, SU1 Pathway A near Diapirs Ci and Cii; Figure 17h). Even when large, stacked channel complexes cross structures without showing substantial topographical influence, such as changes in routing direction or channel geomorphology (e.g. SU5 Pathway E over Salt Walls B, C and D), structures may still control the location of the major avulsion nodes (Figures 14, 17i). Control over the avulsions nodes may be due to a brief tectonic uplift resulting in subtle gradient changes over fold crests (Kolla, 2007), thereby leading the nodes to be located directly above or on the immediate down-dip flank of salt walls. Most of the avulsion nodes occur on the outside of the meander bends due to flow stripping and highest channel instability (Armitage *et al.*, 2012). As flows tend more towards the outer channel bends, this eventually leads to flows cutting through channel confinement and depositing the initial unconfined lobes before a new channel-levee complex successfully or unsuccessfully forms (e.g. Figures 14, 15a). When these unconfined flows encounter little structural influence, lobe stacking patterns may display progradation, backstepping or compensational infill, with a tendency towards compensational stacking (e.g. SU5 Pathway Eii; Figure 17j).

When the structural growth rate and sediment accumulation are more balanced, preservation of the interplay between these two controls may be more subtle, such as control over the CLTZ. The abrupt shallowing of a local gradient controls the CLTZ and locates it immediately down-dip of structural culminations, thereby transitioning from a major channel complex into a large lobe complex (e.g. SU5 Pathway Eii; Figure 17k). Understanding if there is a local gradient change due to subtle structural topography helps to determine if minor channel complexes narrow to a width below seismic resolution or deposited hard-to-image muddier lobes.

Stages of Structural Growth and Evolving Systems

After describing snapshots of static structural topography influencing deep-water systems, we can dynamically define the sea-floor expression of salt-cored structures in three general stages of a typical phase of structural growth, being (i) initiation, (ii) maturity, and (iv) decay or death (Figure 18). These growth stages can be applied to other tectonic settings (e.g. normal fault development), but the details within these stages are particularly unique to the contractional salt domain of a salt-detached slope where diapir squeezing and rejuvenation is a key control for accommodation development. Categorizing the stages within the contractional salt domain is based on observations in the study area and additional studies (e.g. Oluboyo *et al.*, 2014; Rodriguez *et al.*, 2020). The study interval importantly records the maturity through decay stages of salt-cored growth, as many outcrop and seismic studies focus purely on the maturity stage (e.g. Gee & Gawthorpe, 2006; Clark & Cartwright, 2012; Oluboyo *et* *al.*, 2014; Pinter *et al.*, 2018). Spatial variations within the stages is also dependent on structural gradients being sufficient to disrupt the regional depositional gradient. While salt walls within the eastern domain (e.g. Salt Walls A, B, C, D, E), gradually lose their topographical influence over time, the salt walls in the western domain (e.g. Salt Wall Fi, Fii, Diapirs E, Dii, G, salt plateau) are continually blocking or diverting deep-water systems over long distances with segment boundaries and chokepoints acting on fairways linking minibasins, throughout the maturity and decay structural growth stages.

The initiation stage is characterised by the early growth of low relief, segmented salt-cored structures that create minor diversions of channel-lobe systems as the systems are mainly influenced by the regional margin gradient (Figure 18a). The record of geomorphological and sediment routing changes due to minor structurally-controlled sea-floor rugosity may be difficult to recognise as the turbidite systems are mainly through-going across the minibasins. The limited diversions of turbidite systems are due to early formed fold topography. There are few lobe complexes due to a lack of gradient changes and confining minibasins, thereby channel complexes are the most abundant deep-water element during this stage (Figure 18a). The channels move gradually in response to structural growth through lateral migration.

The maturity stage is distinguished by high relief and laterally linked salt-cored highs that are capable of blocking and diverting channel-lobe systems in some minibasins but also create low deposition 'shadow zones' in others (Figure 18b; Oluboyo *et al.*, 2014). Large elongate salt walls separate fully developed minibasins which confine flows and contain mostly axial channel-lobe systems. Segment boundaries and chokepoints developed between structural topographies result in long-lived sediment pathways if sediment accumulation is sufficient, and potentially controls the location of the major CLTZ (Figure 18b). An indirect influence of the high structural relief created during the maturity stage is topographic complexity around localized slumps creating additional degradation of fold flanks (e.g. Figures 10b, c, 18b; Wu *et al.*, 2020). While extensive MTC's on active plate margins have been shown to cause substantial diversions of channel complexes and control avulsion nodes (e.g. Olafiranye *et al.*, 2013; Ortiz-Karpf *et al.*, 2017; Zhao *et al.*, 2019), the MTC's within the study interval are present as relatively small (18 km^2) and thin (c. 40 ms TWTT) slumps sourced from local salt-cored highs. Although the slumps may cause minor diversion of channel complexes, they have a more material impact on channel complex width and sinuosity. Differential compaction of older deposits, such as lobe complexes (e.g. Pathway E; Figure 10a) and channel complexes (e.g. Pathway A_{ii}; Figure 10b, c) also influences sea-floor topography within minibasins, thereby influencing the routing of younger channel complexes. This is topographic influence is possible in the large lobe complex from Pathway D in SU3 (Figure 9).

The final stage, decay or death, contains long linked structures with diminished sea-floor relief due to sediment accumulation outpacing structural growth rate (Figure 18c). Minibasins subside less strongly during this time and are poorly defined by adjacent salt walls, leading to channel complexes crossing over highs that previously blocked or diverted turbidite systems. As sediment accumulation rate is greater than the growth of structures, structural controls on channel-lobe systems is more subtle. During the decay/death stage channel movement may be mostly abrupt via avulsions rather than gradual lateral migration, as gradual diversion is a response of the deep-water systems to actively growing salt-cored structures. Instead, in the decay stage, subtle structural highs control major avulsion nodes along or immediately down-dip of fold flanks due to occasional 'pumping-up' of the salt walls through squeezing (Figure 18c). Differential compaction of thicker minibasin fill (> 200 m burial sensu Ward *et al.*, 2017) along these areas may also play an important role in controlling avulsion node localities through creating gradual gradients. Although most of the salt-cored structures are low relief during this stage, some large structures may be long-lived and continue blocking sediment pathways and ponding sediments (Figure 18c).

CONCLUSIONS

Evolving salt tectonics and corresponding sea-floor topographies along salt-influenced passive margins impacts the routing and geomorphology of submarine channel-lobe systems on a regional-scale.

Mapping the evolution of these systems has helped us to understand the location and character of channel-lobe transitions and avulsion nodes, in relation to sea-floor topography and develop an understanding of deep-water systems during initiation, maturity and death/decay stages of salt-cored folds and minibasin depocentres. A range of geomorphology, stacking and internal architecture of channels, lobes and transitional zones can be understood in terms of the ratio between structural growth rate and sediment accumulation rate.

Five Miocene-aged seismic units are mapped within a series of salt withdrawal minibasins in the Kwanza Basin, offshore Angola. Initially, high relief salt-cored structures confine channel-lobe systems to the up-dip minibasins through large-scale diversion of transverse-to-structure channel complexes, with segment boundaries localising sediment pathways between adjacent axially-trending minibasins. These major structures control the location of channel-lobe transition zones to immediately down-dip of segment boundaries, chokepoints and structural gradient changes across fold hinges. The youngest units only display subtle structural topography and gradually the influence of the salt-cored structures diminishes with time. Low relief structures still influence turbidite systems through small-scale diversion and by controlling the location of avulsion above remnant structural highs. Control over avulsion nodes is likely due to brief periods of minor rejuvenated salt movement during times of dominating sediment accumulation and/or subtle inherited gradients from differential compaction. Channels are therefore moving in response to structural growth abruptly via avulsion nodes, as well as gradually through lateral migration when there is substantial down-dip accommodation and lateral tilting to motivate channel diversion.

The results of this study combined with observations in other salt-influenced margins have allowed us to develop models of the tectono-sedimentary response of deep-water depositional systems to three general stages of structural growth, initiation, maturity and decay or death. The early initiation stage contains low relief, segmented salt-cored structures and poorly defined minibasins, allowing channel complexes to largely follow the regional margin gradient with minimal diversions or ponding of unconfined flows. The maturity stage is characterised by elongate high-relief salt-cored folds, thereby leading to large-scale axial diversion of channel complexes along structural strike towards segment boundaries and chokepoints. Ponded lobe complexes and slumps derived from local fold flanks are also commonly deposited in the well-developed minibasins. Structural relief gradually diminishes with time during the decay/death stage as sediment accumulation begins to once again outpace structural growth. This leads to a more complex array of through-going channel-lobe systems with occasional blocking. The models presented in this paper contribute to the understanding of the alterations to channel-lobe systems during the stages of structural growth and can be applied to similar settings containing salt withdrawal minibasins. The models also explain complications due to strong local structural gradients and the varying angle of incidence between the deep-water system and structural strike, which drastically impacts the degree of blocking and diversion.

ACKNOWLEDGEMENTS

This study is part of the first author's PhD project, which is supported by the Turbidites, Topography and Tectonics (T^3) project funded by Equinor. We especially thank Michal Warchol, Michal Janocko and Frode Hadler-Jacobsen for their thoughtful feedback and discussion over the years. We acknowledge WesternGeco for providing access to the seismic data and giving permission to publish in this paper. We also thank Schlumberger, Eliis and Geoteric for providing software under educational licenses to the 3-D seismic lab at the University of Bergen. Gawthorpe acknowledges VISTA for funding the VISTA Professorship.

REFERENCES

Aas, T.E., Basani, R., Howell, J.A. & Hansen, E. (2014) Forward Modelling as a Method for Predicting the Distribution of Deep-Marine Sands: An Example from the Peira Cava Sub-Basin. *Geological Society, London, Special Publications*, *387*, 247-269.

Abreu, V., Sullivan, M., Pirmez, C. & Mohrig, D. (2003) Lateral Accretion Packages (Laps): An Important Reservoir Element in Deep Water Sinuous Channels. *Marine and Petroleum Geology*, *20*, 631-648.

Anderson, J.E., Cartwright, J., Drysdall, S.J. & Vivian, N. (2000) Controls on Turbidite Sand Deposition During Gravity-Driven Extension of a Passive Margin: Examples from Miocene Sediments in Block 4, Angola. *Marine and Petroleum Geology*, *17*, 1165-1203.

Armitage, D.A., Mchargue, T., Fildani, A. & Graham, S.A. (2012) Postavulsion Channel Evolution: Niger Delta Continental Slope. *AAPG Bulletin*, *96*, 823-843.

Banham, S.G. & Mountney, N.P. (2013) Evolution of Fluvial Systems in Salt-Walled Mini-Basins: A Review and New Insights. *Sedimentary Geology*, *296*, 142-166.

Basani, R., Janocko, M., Cartigny, M.J.B., Hansen, E.W.M. & Eggenhuisen, J.T. (2014) Massflow-3d as a Simulation Tool for Turbidity Currents: Some Preliminary Results. In: *From Depositional Systems to Sedimentary Successions on the Norwegian Continental Margin* (Ed. by A. W. Martinius, R. Ravnas, J. A. Howell, R. J. Steel & J. P. Wonham), *46*, 587-608. IAS Special Publication.

Brice, S.E., Cochran, M.D., Pardo, G. & Edwards, A.D. (1982) *Tectonics and Sedimentation of the South Atlantic Rift Sequence: Cabinda, Angola: Rifted Margins: Field Investigations of Margin Structure and Stratigraphy*.

Brooks, H., Hodgson, D., Brunt, R.L., Peakall, J., Hofstra & Flint, S. (2018) Deep-Water Channel-Lobe Transition Zone Dynamics: Processes and Depositional Architecture, an Example from the Karoo Basin, South Africa. *GSA Bulletin*, *130*, 1723-1746.

Broucke, O., Temple, F., Rouby, D., Robin, C., Calassou, S., Nalpas, T. & Guillocheau, F. (2004) The Role of Deformation Processes on the Geometry of Mud-Dominated Turbiditic Systems, Oligocene and Lower-Middle Miocene of the Lower Congo Basin (West African Margin). *Marine and Petroleum Geology*, *21*, 327-348.

Brown, A.R. (1999) *Interpretation of Three-Dimensional Seismic Data*, Tulsa, Oklahoma.

Brownfield, M.E. & Charpentier, R.R. (2006) Geology and Total Petroleum Systems of the West-Central Coastal Province (7203), West Africa *U.S. Geological Survey Bulletin 2207-B*, 52 p.

Brun, J.-P. & Fort, X. (2011) Salt Tectonics at Passive Margins: Geology Versus Models. *Marine and Petroleum Geology*, *28*, 1123-1145.

Bull, S., Cartwright, J. & Huuse, M. (2009) A Review of Kinematic Indicators from Mass-Transport Complexes Using 3d Seismic Data. *Marine and Petroleum Geology*, *26*, 1132-1151.

Cartigny, M.J.B., Eggenhuisen, J.T., Hansen, E.W.M. & Postma, G. (2013) Concentration-Dependent Flow Stratification in Experimental High-Density Turbidity Currents and Their Relevance to Turbidite Facies Models. *Journal of Sedimentary Research*, *83*, 1046-1064.

Clark, I.R. & Cartwright, J.A. (2009) Interactions between Submarine Channel Systems and Deformation in Deepwater Fold Belts: Examples from the Levant Basin, Eastern Mediterranean Sea. *Marine and Petroleum Geology*, *26*, 1465-1482.

Clark, I.R. & Cartwright, J.a. (2012) Interactions between Coeval Sedimentation and Deformation from the Niger Delta Deepwater Fold Belt. *SEPM Special Publication*, 243-267.

Collinson, J.D. & Thompson, D.B. (1982) *Sedimentary Structures*.

Deptuck, M.E., Steffens, G.S., Barton, M. & Pirmez, C. (2003) Architecture and Evolution of Upper Fan Channel-Belts on the Niger Delta Slope and in the Arabian Sea. *Marine and Petroleum Geology*, *20*, 649-676.

Deptuck, M.E., Sylvester, Z., Pirmez, C. & O'byrne, C. (2007) Migration–Aggradation History and 3-D Seismic Geomorphology of Submarine Channels in the Pleistocene Benin-Major Canyon, Western Niger Delta Slope. *Marine and Petroleum Geology*, *24*, 406-433.

Doughty-Jones, G., Mayall, M. & Lonergan, L. (2017) Stratigraphy, Facies, and Evolution of Deep-Water Lobe Complexes within a Salt-Controlled Intraslope Minibasin. *AAPG Bulletin*, *101*, 1879-1904.

Doughty-Jones, G., Lonergan, L., Mayall, M. & Dee, S. (2019) The Role of Structural Growth in Controlling the Facies and Distribution of Mass Transport Deposits in a Deep-Water Salt Minbasin. *Marine and Petroleum Geology*.

Duval, B., Cramez, C. & Jackson, M.P.A. (1992) Raft Tectonics in the Kwanza Basin, Angola. *Marine and Petroleum Geology*, *9*, 389-404.

Eggenhuisen, J.T. & Mccaffrey, W.D. (2012) The Vertical Turbulence Structure of Experimental Turbidity Currents Encountering Basal Obstructions: Implications for Vertical Suspended Sediment Distribution in Non-Equilibrium Currents. *Sedimentology*, *59*, 1101-1120.

Fort, X., Brun, J.P. & Chauvel, F. (2004) Salt Tectonics on the Angolan Margin, Synsedimentary Deformation Processes. *AAPG Bulletin*, *88*, 1523-1544.

Gamberi, F. & Rovere, M. (2011) Architecture of a Modern Transient Slope Fan (Villafranca Fan, Gioia Basin-Southeastern Tyrrhenian Sea). *Sedimentary Geology*, *236*, 211-225.

Gamboa, D. & Alves, T.M. (2015) Spatial and Dimensional Relationships of Submarine Slope Architectural Elements: A Seismic-Scale Analysis from the Espírito Santo Basin (SE Brazil). *Marine and Petroleum Geology*, *64*, 43-57.

Gawthorpe, R. L., Fraser, A. J., & Collier, R. E. L. (1994). Sequence stratigraphy in active extensional basins: implications for the interpretation of ancient basin-fills. *Marine and Petroleum geology*, *11*, 642-658.

Gawthorpe, R.L. & Leeder, M.R. (2000) Tectono-Sedimentary Evolution of Active Extensional Basins. *Basin Research*, *12*, 195-218.

Ge, Z., Nemec, W., Gawthorpe, R.L., Rotevatn, A. & Hansen, E.W.M. (2018) Response of Unconfined Turbidity Current to Relay-Ramp Topography: Insights from Process-Based Numerical Modelling. *Basin Research*, *30*, 321-343.

Gee, M.J.R. & Gawthorpe, R.L. (2006) Submarine Channels Controlled by Salt Tectonics: Examples from 3d Seismic Data Offshore Angola. *Marine and Petroleum Geology*, *23*, 443-458.

Gee, M.J.R., Gawthorpe, R.L., Bakke, K. & Friedmann, S.J. (2007) Seismic Geomorphology and Evolution of Submarine Channels from the Angolan Continental Margin. *Journal of Sedimentary Research*, *77*, 433-446.

Giles, K.A. & Rowan, M.G. (2012) Concepts in Halokinetic-Sequence Deformation and Stratigraphy. *Geological Society, London, Special Publications*, *363*, 7-31.

Guiraud, M., Buta-Neto, A. & Quesne, D. (2010) Segmentation and Differential Post-Rift Uplift at the Angola Margin as Recorded by the Transform-Rifted Benguela and Oblique-to-Orthogonal-Rifted Kwanza Basins. *Marine and Petroleum Geology*, *27*, 1040-1068.

Guiraud, R. & Maurin, J.C. (1992) Early Cretaceous Rifts of Western and Central Africa: An Overview. *Tectonophysics*, *213*, 153-168.

Hadler-Jacobsen, F., Johannessen, E.P., Ashton, N., Henriksen, S., Johnson, S.D. & Kristensen, J.B. (2005) Submarine Fan Morphology and Lithology Distribution: A Predictable Function of Sediment Delivery, Gross Shelf-to-Basin Relief, Slope Gradient and Basin Topography. In *Geological Society, London, Petroleum Geology Conference series*, *6*, 1121-1146.

Hadler-Jacobsen, F., Gardner, M.H. & Borer, J.M. (2007) Seismic Stratigraphic and Geomorphic Analysis of Deep-Marine Deposition Along the West African Continental Margin. *Geological Society, London, Special Publication*, *277*, 47-84.

Hansen, L., Janocko, M., Kane, I. & Kneller, B. (2017) Submarine Channel Evolution, Terrace Development, and Preservation of Intra-Channel Thin-Bedded Turbidites: Mahin and Avon Channels, Offshore Nigeria. *Marine Geology*, *383*, 146-167.

Haughton, P.D.W. (2000) Evolving Turbidite Systems on a Deforming Basin Floor, Tabernas, SE Spain. *Sedimentology*, *47*, 497-518.

Hay, D.C. (2012) Stratigraphic Evolution of a Tortuous Corridor from the Stepped Slope of Angola. *Application of the principles of seismic geomorphology to continental slope and base-of-slope* *systems: Case studies from sea floor and near–sea floor analogs: SEPM Special Publication*, *99*, 163-180.

Hofstra, M., Hodgson, D.M., Peakall, J. & Flint, S.S. (2015) Giant Scour-Fills in Ancient Channel-Lobe Transition Zones: Formative Processes and Depositional Architecture. *Sedimentary Geology*, *329*, 98-114.

Howlett, D.M., Ge, Z., Nemec, W., Gawthorpe, R.L., Rotevatn, A. & Jackson, C.A.L. (2019) Response of Unconfined Turbidity Current to Deep-Water Fold and Thrust Belt Topography: Orthogonal Incidence on Solitary and Segmented Folds. *Sedimentology, 66,* 2425-2454.

Huang, Y. & Zheng, L. (2019) Hydrocarbon Accumulation in Deep Water Areas of Angola in West Africa. *Petroleum Research*, *4*, 268-275.

Hudec, M.R. & Jackson, M.P. (2002) Structural Segmentation, Inversion, and Salt Tectonics on a Passive Margin: Evolution of the Inner Kwanza Basin, Angola. *GSA Bulletin*, *114*, 1222-1244.

Hudec, M.R. & Jackson, M.P.A. (2004) Regional Restoration across the Kwanza Basin, Angola: Salt Tectonics Triggered by Repeated Uplift of a Metastable Passive Margin. *AAPG Bulletin*, *88*, 971-990.

Hudec, M.R. & Jackson, M.P.A. (2007) Terra Infirma: Understanding Salt Tectonics. *Earth-Science Reviews*, *82*, 1-28.

Jackson, C.A.L. & Lewis, M.M. (2012) Origin of an Anhydrite Sheath Encircling a Salt Diapir and Implications for the Seismic Imaging of Steep-Sided Salt Structures, Egersund Basin, Northern North Sea. *Journal of the Geological Society*, *169*, 593-599.

Jackson, C.A.L., Rodriguez, C.R., Rotevatn, A. & Bell, R.E. (2014) Geological and Geophysical Expression of a Primary Salt Weld: An Example from the Santos Basin, Brazil. *Interpretation*, *2*, SM77-SM89.

Jackson, M.P.A., Hudec, M.R. & Hegarty, K.A. (2005) The Great West African Tertiary Coastal Uplift: Fact or Fiction? A Perspective from the Angolan Divergent Margin. *Tectonics*, *24*, 1-23.

Janocko, M., Nemec, W., Henriksen, S. & Warcho, M. (2013) The Diversity of Deep-Water Sinuous Channel Belts and Slope Valley-Fill Complexes. *Marine and Petroleum Geology*, *41*, 7-34.

Jian-Ping, L.I.U., Pan, X.H., Jun, M., Tian, Z.J. & Chen, Y.J.W., L. K. (2008) Petroleum Geology and Resources in West Africa: An Overview. *Petroleum Exploration and Development*, *35*, 378-383.

Jobe, Z.R., Sylvester, Z., Parker, A.O., Howes, N., Slowey, N. & Pirmez, C. (2015) Rapid Adjustment of Submarine Channel Architecture to Changes in Sediment Supply. *Journal of Sedimentary Research*, *85*, 729-753.

Jones, I.F. & Davison, I. (2014) Seismic Imaging in and around Salt Bodies. *Interpretation*, *2*, SL1-SL20.

Karner, G.D. & Driscoll, N.W. (1999) Tectonic and Stratigraphic Development of the West African and Eastern Brazilian Margins: Insights from Quantitative Basin Modelling. *Geological Society London Special Publication*, *153*, 11-40.

Kneller, B., Edwards, D., Mccaffrey, W. & Moore, R. (1991) Oblique Reflection of Turbidity Currents. *Geology*, *19*, 250-252.

Kneller, B. (1995) Beyond the Turbidite Paradigm: Physical Models for Deposition of Turbidites and Their Implications for Reservoir Prediction. *Geological Society London Special Publication*, *94*, 31-49.

Kneller, B.C. & Mccaffrey, W.D. (1995) Modelling the Effects of Salt-Induced Topography on Deposition from Turbidity Currents. *Salt, sediment and hydrocarbons: Gulf Coast Section SEPM*, *1*, 137-145.

Kolla, V. (2007) A Review of Sinuous Channel Avulsion Patterns in Some Major Deep-Seafans and Factors Controlling Them. *Marine and Petroleum Geology*, *24*, 450–469.

Lavier, L.L., Steckler, M.S. & Brigaud, F. (2001) Climatic and Tectonic Control on the Cenozoic Evolution of the West African Margin. *Marine Geology*, *178*, 63-80.

Lundin, E.R. (1992) Thin-Skinned Extensional Tectonics on a Salt Detachment, Northern Kwanza Basin, Angola. *Marine and Petroleum Geology*, *9*, 405-411.

Maestrelli, D., Iacopini, D., Jihad, A.A., Bond, C.E. & Bonini, M. (2017) Seismic and Structural Characterization of Fluid Escape Pipes Using 3d and Partial Stack Seismic from the Loyal Field (Scotland, UK): A Multiphase and Repeated Intrusive Mechanism. *Marine and Petroleum Geology*, *88*, 489-510.

Maier, K.L., Fildani, A., Mchargue, T.R., Paull, C.K., Graham, S.A. & Caress, D.W. (2012) Punctuated Deep-Water Channel Migration: High-Resolution Subsurface Data from the Lucia Chica Channel System, Offshore California, U.S.A. *Journal of Sedimentary Research*, *82*, 1-8.

Martinez, J.F., Cartwright, J. & Hall, B. (2005) 3d Seismic Interpretation of Slump Complexes: Examples from the Continental Margin of Israel. *Basin Research*, *17*, 83-108.

Marton, L.G. (2000) Evolution of the Angolan Passive Margin, West Africa, with Emphasis on Post-Salt Structural Styles. *Geophysical Monograph-American Geophysical Union*, *115*, 129–149.

Mattos, N.H., Alves, T.M. & Scully, A. (2019) Structural and Depositional Controls on Plio-Pleistocene Submarine Channel Geometry (Taranaki Basin, New Zealand). *Basin Research*, *31*, 136-154.

Mayall, M., Lonergan, L., Bowman, A., James, S., Mills, K., Primmer, T., Pope, D., Rogers, L. & Skeene, R. (2010) The Response of Turbidite Slope Channels to Growth-Induced Seabed Topography. *AAPG Bulletin*, *94*, 1011-1030.

Mcardle, N.J. & Ackers, M.A. (2012) Understanding Seismic Thin-Bed Responses Using Frequency Decomposition and Rgb Blending. *First Break*, *30*, 57-65.

Mchargue, T., Hodgson, D. & Shelef, E. (2020 PREPRINT) Architectural Diversity of Submarine Unconfined Lobate Deposits.

Moulin, M., Aslanian, D., Olivet, J.-L., Contrucci, I., Matias, L., Géli, L., Klingelhoefer, F., Nouzé, H., Réhault, J.-P. & Unternehr, P. (2005) Geological Constraints on the Evolution of the Angolan Margin Based on Reflection and Refraction Seismic Data (Zaïango Project). *Geophysical Journal International*, *162*, 793-810.

Muravchik, M., Henstra, G.A., Eliassen, G.T., Gawthorpe, R.L., Leeder, M., Kranis, H., Skourtsos, E. & Andrews, J. (2019) Deep-Water Sediment Transport Patterns and Basin Floor Topography in Early Rift Basins: Plio-Pleistocene Syn-Rift of the Corinth Rift, Greece. *Basin Research, 0,* 1-29.

Niyazia, Y., Eruteya, O.E., Omosanya, K.O., Harishidayat, D., Johansen, S.E. & Waldmann, N. (2018) Seismic Geomorphology of Submarine Channel-Belt Complexes in Thepliocene of the Levant Basin, Offshore Central Israel. *Marine Geology*, *403*, 123-128.

Olafiranye, K., Jackson, C.A.L. & Hodgson, D.M. (2013) The Role of Tectonics and Mass-Transport Complex Emplacement on Upper Slope Stratigraphic Evolution: A 3d Seismic Case Study from Offshore Angola. *Marine and Petroleum Geology*, *44*, 196-216.

Oluboyo, A.P., Gawthorpe, R.L., Bakke, K. & Hadler-Jacobsen, F. (2014) Salt Tectonic Controls on Deep-Water Turbidite Depositional Systems: Miocene, Southwestern Lower Congo Basin, Offshore Angola. *Basin Research*, *26*, 597-620.

Ortiz-Karpf, A., Hodgson, D.M. & Mccaffrey, W.D. (2015) The Role of Mass-Transport Complexes in Controlling Channel Avulsion and the Subsequent Sediment Dispersal Patterns on an Active Margin: The Magdalena Fan, Offshore Colombia. *Marine and Petroleum Geology*, *64*, 58-75.

Ortiz-Karpf, A., Hodgson, D.M., Jackson, C.A.L. & Mccaffrey, W.D. (2017) Influence of Seabed Morphology and Substrate Composition on Mass-Transport Flow Processes and Pathways: Insights from the Magdalena Fan, Offshore Colombia. *Journal of Sedimentary Research*, *87*, 189-209.

Othman, A.A.A., Fathy, M. & Maher, A. (2016) Use of Spectral Decomposition Technique for Delineation of Channels at Solar Gas Discovery, Offshore West Nile Delta, Egypt. *Egyptian Journal of Petroleum*, *25*, 45-51.

Patacci, M., Haughton, P.D.W. & Mccaffrey, W.D. (2015) Flow Behavior of Ponded Turbidity Currents. *Journal of Sedimentary Research*, *85*, 885-902.

Peel, F.J. (2014) The Engines of Gravity-Driven Movement on Passive Margins: Quantifying the Relative Contribution of Spreading vs. Gravity Sliding Mechanisms. *Tectonophysics*, *633*, 126-142.

Pichel, L.M., Peel, F., Jackson, C.A.L. & Huuse, M. (2018) Geometry and Kinematics of Salt-Detached Ramp Syncline Basins. *Journal of Structural Geology*, *115*, 208-230.

Pinter, P.R., Butler, R.W.H., Hartley, A.J., Maniscalco, R., Baldassini, N. & Di Stefano, A. (2018) Tracking Sand-Fairways through a Deformed Turbidite System: The Numidian (Miocene) of Central Sicily, Italy. *Basin Research*, *30*, 480-501.

Pirmez, C., Hiscou, R.N. & Kronen, J.K. (1997) Sandy Turbidite Successions at the Base of Channel-Levee Systems of the Amazon Fan Revealed by Fms Logs and Cores: Unraveling the Facies Architecture of Large Submarine Fans. In: *Proceedings-Ocean Drilling Program Scientific Results, 155*, 7-34.

Posamentier, H.W. (2003) Depositional Elements Associated with a Basin Floor Channel-Levee System: Case Study from the Gulf of Mexico. *Marine and Petroleum Geology*, *20*, 677-690.

Posamentier, H.W. & Kolla, V. (2003) Seismic Geomorphology and Stratigraphy of Depositional Elements in Deep-Water Settings. *Journal of Sedimentary Research*, *73*, 367-388.

Prather, B., Booth, J., Steffens, G. & Craig, P. (1998) Classification, Lithologic Calibration, and Stratigraphic Succession of Seismic Facies of Intraslope Basins, Deep-Water Gulf of Mexico. *AAPG Bulletin*, *82*, 701-728.

Prather, B.E., Pirmez, C., Sylvester, Z. & Prather, D.S. (2012) Stratigraphic Response to Evolving Geomorphology in a Submarine Apron Perched on the Upper Niger Delta Slope. *Application of the Principles of Seismic Geomorphology to Continental-Slope and Base-of-Slope Systems: Case Studies from Seafloor and Near-Seafloor Analogues*, *Society for Sedimentary Geology (SEPM) Special Publication, 99,* 145-161.

Quirk, D.G., Schødt, N., Lassen, B., Ings, S.J., Hsu, D., Hirsch, K.K. & Von Nicolai, C. (2012) Salt Tectonics on Passive Margins: Examples from Santos, Campos and Kwanza Basins. *Geological Society, London, Special Publications*, *363*, 207-244.

Ravnås, R. & Steel, R.J. (1998) Architecture of Marine Rift-Basin Successions. *AAPG Bulletin*, *82*, 110-146.

Rodriguez, C.R., Jackson, C.A.L., Bell, R.E., Rotevatn, A. & Francis, M. (2020 PREPRINT) Deep-Water Reservoir Distribution on a Salt-Influenced Slope, Santos Basin, Offshore Brazil.

Rojo, L.A. & Escalona, A. (2018) Controls on Minibasin Infill in the Nordkapp Basin: Evidence of Complex Triassic Synsedimentary Deposition Influenced by Salt Tectonics. *AAPG Bulletin*, *102*, 1239-1272.

Smith, R.U. (2004) Silled Sub-Basins to Connected Tortuous Corridors: Sediment Distribution Systems on Topographically Complex Sub-Aqueous Slopes. *Geological Society, London, Special Publication*, *222*, 23-44.

Straub, K.M. & Mohrig, D. (2009) Constructional Canyons Built by Sheet-Like Turbidity Currents: Observations from Offshore Brunei Darussalam. *Journal of Sedimentary Research*, *79*, 24-39.

Tari, G., Molnar, J. & Ashton, N. (2003) Examples of Salt Tectonics from West Africa: A Comparative Approach. *Geological Society, London, Special Publication*, *207*, 85-104.

Tinterri, R., Laporta, M. & Ogata, K. (2017) Asymmetrical Cross-Current Turbidite Facies Tract in a Structurally-Confined Mini-Basin (Priabonian-Rupelian, Ranzano Sandstone, Northern Apennines, Italy). *Sedimentary Geology*, *352*, 63-87.

Valle, P.J., Gjelberg, J.G. & Helland-Hansen, W. (2001) Tectonostratigraphic Development in the Esatern Lower Congo, Basin, Offshore Angola, West Africa. *Marine and Petroleum Geology*, *18*, 909-927.

Van Andel, T.H. & Komar, P.D. (1969) Ponded Sediments of the Mid-Atlantic Ridge between 22 and 23 North Latitude. *Geological Society of America Bulletin*, *80*, 1163-1190.

Ward, N.I.P., Alves, T.M. & Blenkinsop, T.G. (2017) Differential Compaction over Late Miocene Submarine Channels in Se Brazil: Implications for Trap Formation. *GSA Bulletin*, *130*, 208-221.

Wu, N., Jackson, C.A.L., Johnson, H.D., Hodgson, D.M. & Nugraha, H.D. (2020) Mass-Transport Complexes (MTCs) Document Subsidence Patterns in a Northern Gulf of Mexico Salt Minibasin. *Basin Research*.

Zhao, X., Qi, K., Patacci, M., Tan, C. & Xie, T. (2019) Submarine Channel Network Evolution above an Extensive Mass-Transport Complex: A 3d Seismic Case Study from the Niger Delta Continental Slope. *Marine and Petroleum Geology*, *104*, 231-248.

FIGURE CAPTIONS

Figure 1 (a) Simplified contractional salt domains in the Kwanza Basin, Angola with the study area outlined (modified after Hudec & Jackson, 2004; additions from Tari *et al*., 2003; Serié *et al.*, 2017). (b) Geological cross-section showing the regional tectono-stratigraphic framework through the Kwanza Basin (from Hudec & Jackson, 2004). The study area is within the contractional domain containing salt-cored structures such as salt stocks ('diapirs') and salt walls up-dip, and a thickened salt plateau down-dip. Within this area the Miocene is thick in the east and thins westwards onto the thickened salt.

Figure 2 Simplified Upper Jurassic to Quaternary stratigraphy of the Kwanza Basin and main tectonic events (modified after Serié *et al.*, 2017). Note the multiple events reviving salt translation. The five seismic units with corresponding seismic character are displayed on the right-hand side.

Figure 3 (a) Oblique 3-D perspective view of the topography along the present-day sea-floor with corresponding seismic cross-sections shown in Figure 4. Dominant salt-cored structures are outlined in white. The study area can be divided into the eastern domain (elongated co-linear salt walls and minibasins), western domain (segmented and isolated salt-cored structures) and thickened salt plateau. Note how pockmarks (circular negative relief) are largely restricted to the eastern domain and are commonly upflank of salt walls, surrounding diapirs or following high sinuosity stacked Miocene turbidite channels. The trimmed pseudo outcrop relief seismic cross-section displays post-salt minibasin infill. MB = minibasin; SW = salt wall; i, ii, iii represent separate segments of a minibasin or salt-cored structure. (b) Oblique 3-D perspective view of the top salt draped with the relative thickness of salt within the study area, juxtaposed with a pseudo outcrop relief seismic cross-section displaying top and base salt. VE (vertical exaggeration) = 3.

Figure 4 Representative seismic sections with interpretations across the study area displaying the structural and stratigraphic framework for the study (see Figure 3 for cross-section locations). (a) Uninterpreted and interpreted seismic cross-section perpendicular to structural strike illustrating the structural style and variability across the minibasins within the study area. (b) Uninterpreted and interpreted seismic cross-section parallel to structural strike outlining the stratigraphic interval of interest. (c) *(Left)* Inset of interpreted seismic cross-section from (b) to highlight the thickness variations between the five seismic units within the study interval. *(Right)* Simplified map of main salt structures outlined in Figure 3.

Figure 5 Time-thickness maps for the seismic units outlining the spatial evolution of the unit thicks within (a) SU1 (oldest unit), (b) SU2, (c) SU3, (d) SU4, and (e) SU5 (youngest unit). See text for detailed descriptions.

Figure 6 Representative seismic geomorphology for the oldest unit, SU1. (a) Representative spectral decomposition attribute map for SU1 with main salt structures and minibasins labelled. (b) Simplified map of the main submarine channels and lobes for SU1. Older systems are lighter colours, while younger systems are darker colours. Active/positive topographic relief of the salt structures is displayed in solid grey and the inactive/negligible topographic relief is outlined with dashed lines. The major sediment input pathways (A and B) are marked with green arrows. See text for a detailed description of the unit’s evolution.

Figure 7 Representative seismic geomorphology for SU2. (a) Representative spectral decomposition attribute map for SU2 with main salt structures and minibasins labelled. (b) Simplified map of the main submarine channels and lobes for SU2. Older systems are lighter colours, while younger systems are darker colours. Active/positive topographic relief of the salt structures is displayed in solid grey and the inactive/negligible topographic relief is outlined with dashed lines. The major sediment input pathway (C) is marked with a green arrow. See text for a detailed description of the unit’s evolution.

Figure 8 Seismic cross-sections highlighting Pathway C in SU3 (see Figure 7 for positions on map). (a) Near sediment input entry point, (b) crossing over Salt Wall D where there are potentially numerous minor avulsions westwards of small channel complexes, (c) down-dip of Salt Wall Fiii and Diapir F, (d) through high sinuosity and relatively undisturbed channels in MB5, and (e) through low sinuosity channels with no levees closer to Salt Wall Fi. *(Right)* The attribute map displays the high sinuosity channels entering the study area and the location of avulsion nodes on the outer meander bends. Small channel complexes are avulsed northwards and westwards.

Figure 9 Representative seismic geomorphology for SU3. (a) Representative spectral decomposition attribute map for SU3 with main salt structures and minibasins labelled. (b) Simplified map of the main submarine channels and lobes for SU3. Older systems are lighter colours, while younger systems are darker colours. Active/positive topographic relief of the salt structures is displayed in solid grey and the inactive/negligible topographic relief is outlined with dashed lines. The major sediment input pathways (A, B and D) are marked with green arrows. See text for a detailed description of the unit's evolution.

Figure 10 (a) *(Right)* Interpreted proximal to distal seismic cross-sections through Pathway E's large SW-trending lobe complex in SU3. The lobe complex is divided into Di, Dii and Diii (oldest to youngest) based on seismic character and channelisation. *(Left)* Oblique view of the attribute maps for the three lobe complexes displaying shifting lobes and trunk channels. Exaggerated vertical scale. (b) Uninterpreted and interpreted RGB blends from SU3 (see Figure 9 for position on map) outlining the slump derived from Diapir E and the corresponding influence on a channel complex (e.g. decreased sinuosity and meander belt width). A small avulsed channel crosses the slump topography before decreasing below seismic resolution. (c) Interpreted seismic cross-section showing the seismic character of the slump and a decreasing thickness towards the deposit edges (see (b) or Figure 9 for position on map).

Figure 11 Representative seismic geomorphology for SU4. (a) Representative spectral decomposition attribute map for SU4 with main salt structures and minibasins labelled. (b) Simplified map of the main submarine channels and lobes for SU4. Older systems are lighter colours, while younger systems are darker colours. Active/positive topographic relief of the salt structures is displayed in solid grey and the inactive/negligible topographic relief is outlined with dashed lines. The major sediment input pathways (A, B and E) are marked with green arrows. See text for a detailed description of the unit's evolution.

Figure 12 Interpreted seismic cross-sections displaying changing channel geomorphology (e.g. channel width, erosional depth) along the 'chokepoint' between Salt Wall Fi and Diapir G within SU4 (see Figure 11 for position on map). Transitioning from (a) proximal channels, 6 km up-flow of chokepoint, to (b) 1 km up-flow of chokepoint, to (c) narrow chokepoint, to (d) channel-lobe transition, and finally to (e) distal down-flow lobes.

Figure 13 Uninterpreted and interpreted attribute maps showing changing channel morphology (e.g. sinuosity, meander belt width) as a channel complex is gradually diverted into accommodation down-dip of Salt Wall D within SU4 (see Figure 11 for position on map). The channel complex evolves from (c) initially a low gradient and high sinuosity system to (b) a high sinuosity system with wide meander belts in the accommodation down-dip of the salt wall, and finally to (a) a lower sinuosity system closer to a higher relief portion of the salt wall before exiting the study area.

Figure 14 Representative seismic geomorphology for the youngest unit, SU5. (a) Representative spectral decomposition attribute map for SU5 with main salt structures and minibasins labelled. (b) Simplified map of the main submarine channels and lobes for SU5. Older systems are lighter colours, while younger systems are darker colours. Active/positive topographic relief of the salt structures is displayed in solid grey and the inactive/negligible topographic relief is outlined with dashed lines. The major sediment input pathway (E) is marked with a green arrow. See text for a detailed description of the unit's evolution.

Figure 15 Uninterpreted and interpreted seismic cross-sections showing the two main channel complex types within SU5 (see Figure 14 for position on map). (a) Architecture of a stacked channel system along Pathway E with internal slumps, LAPs and internal/external levees, and (b) a deeply erosive meandering channel system surrounded by low amplitude flat-topped terraces.

Figure 16 Pathway evolution between (a) the oldest pathways within SU1 and SU2, (b) SU2 and SU3, (c) SU3 and SU4, and (d) the youngest pathways within SU4 and SU5.

Figure 17 Summary graph of the major observed influences of salt-cored structures on deep-water depositional systems. The x-axis varies from a high rate of structural relief development relative to sediment accumulation on the left side (similar to SU1), to a low rate of structural relief development relative to sedimentation accumulation on the right side (similar to SU5). The y-axis is separated into channels (top) transitioning into channel-lobe transition zones or avulsion nodes (middle) through to lobes (bottom). Each sketch box contains selected reference examples: 1 (Oluboyo et al., 2014), 2 (Mayall et al., 2010), 3 (Gee & Gawthorpe, 2006), 4 (Clark & Cartwright, 2009; 2011), 5 (Hay et al., 2012), 6 (Doughty-Jones et al., 2017).

Figure 18 Dynamic evolution of submarine channel-lobe systems and salt-cored structures within the contractional salt domain from the (a) initiation or development stage, largely controlled by the regional margin gradient and consisting of segmented salt-cored structures, to the (b) maturity stage, comprised of linked high relief salt-cored structures and well-defined minibasins, and finally to the (c) decay or death stage where many structures have substantially diminished in length and relief relative to sedimentation rate. See text for more detailed descriptions.

TABLE CAPTIONS

Table 1 Characteristics of bounding horizons for each seismic unit and internal reflector geometries.

Table 2 Dominate seismic facies within the Miocene as observed in cross-section and on seismic attribute (spectral decomposition-RGB blend) maps.

1161 Figure 1

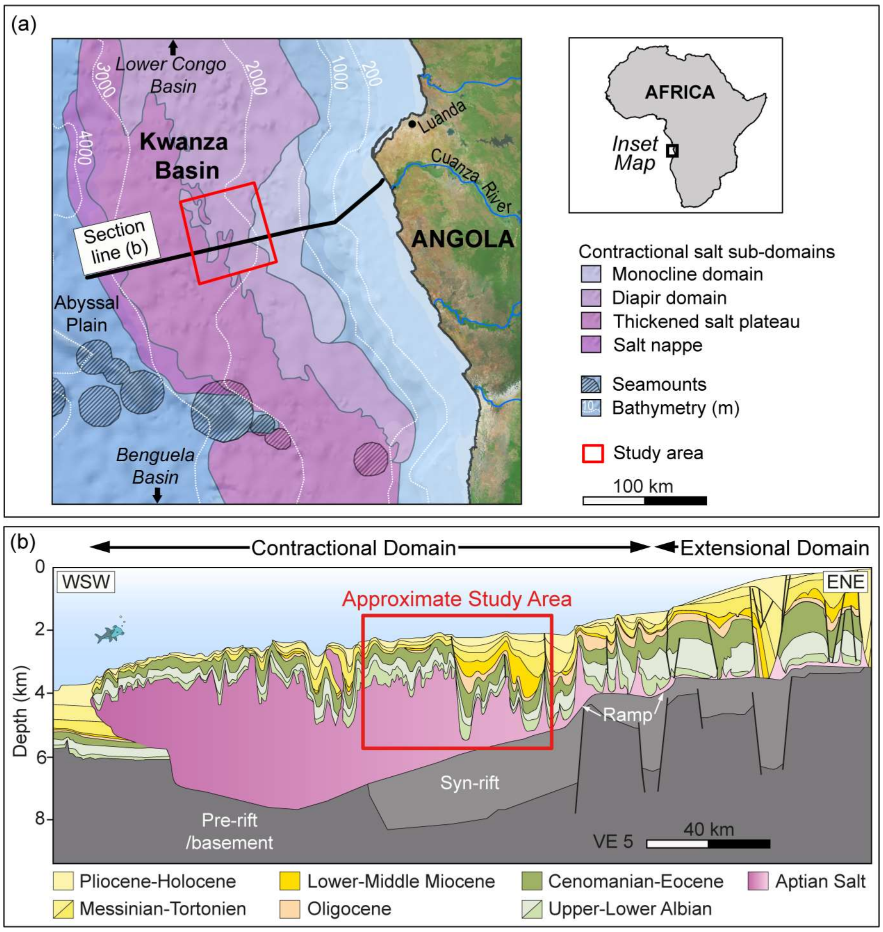

1162

Figure 2

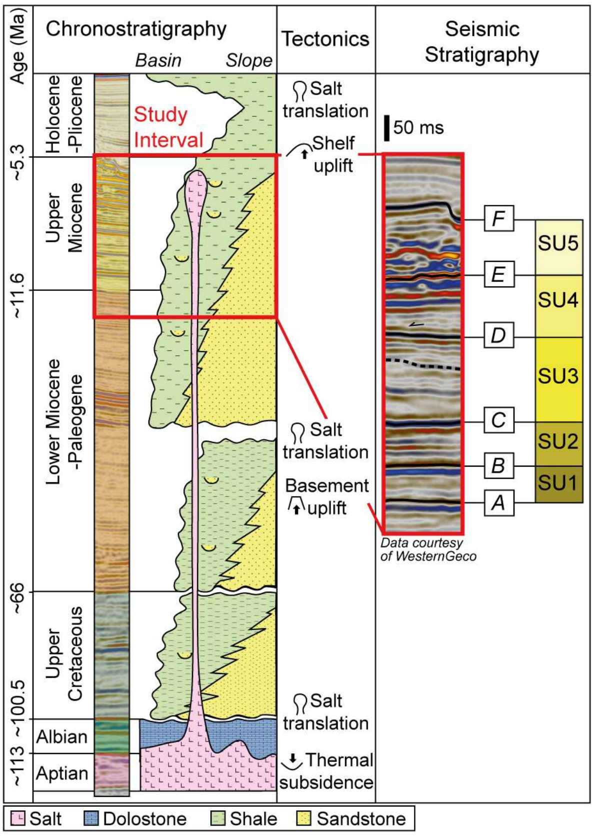
Age (Ma)
Chronostratigraphy
Basin
Slope
Tectonics
Seismic Stratigraphy
Holocene -Pliocene
Study Interval
Salt translation
Shelf uplift
50 ms
~5.3
Upper Miocene
~11.6
F
E
D
C
B
A
SU5
SU4
SU3
SU2
SU1
Lower Miocene -Paleogene
Salt translation
Basement uplift
Data courtesy of WesternGeco
~66
Upper Cretaceous
~100.5
Albian
~113
Aptian
Salt translation
Thermal subsidence
Salt
Dolostone
Shale
Sandstone

1165 Figure 3

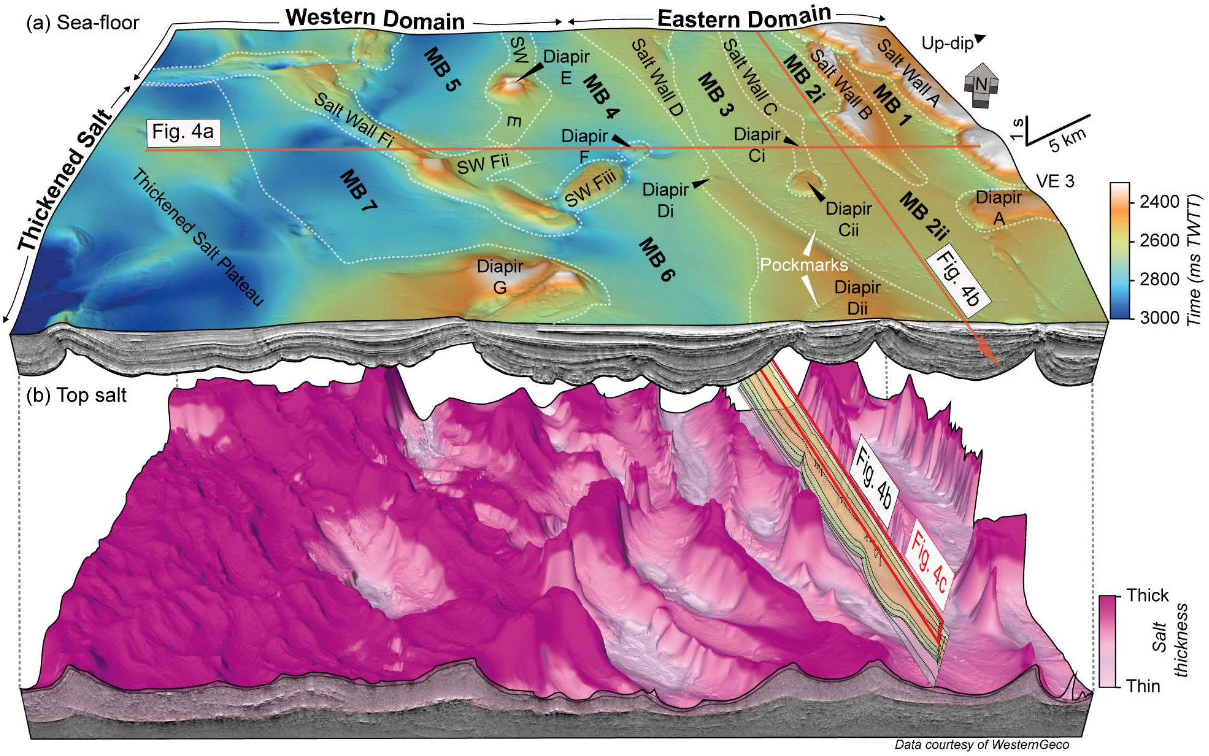

1166

1167 Figure 4

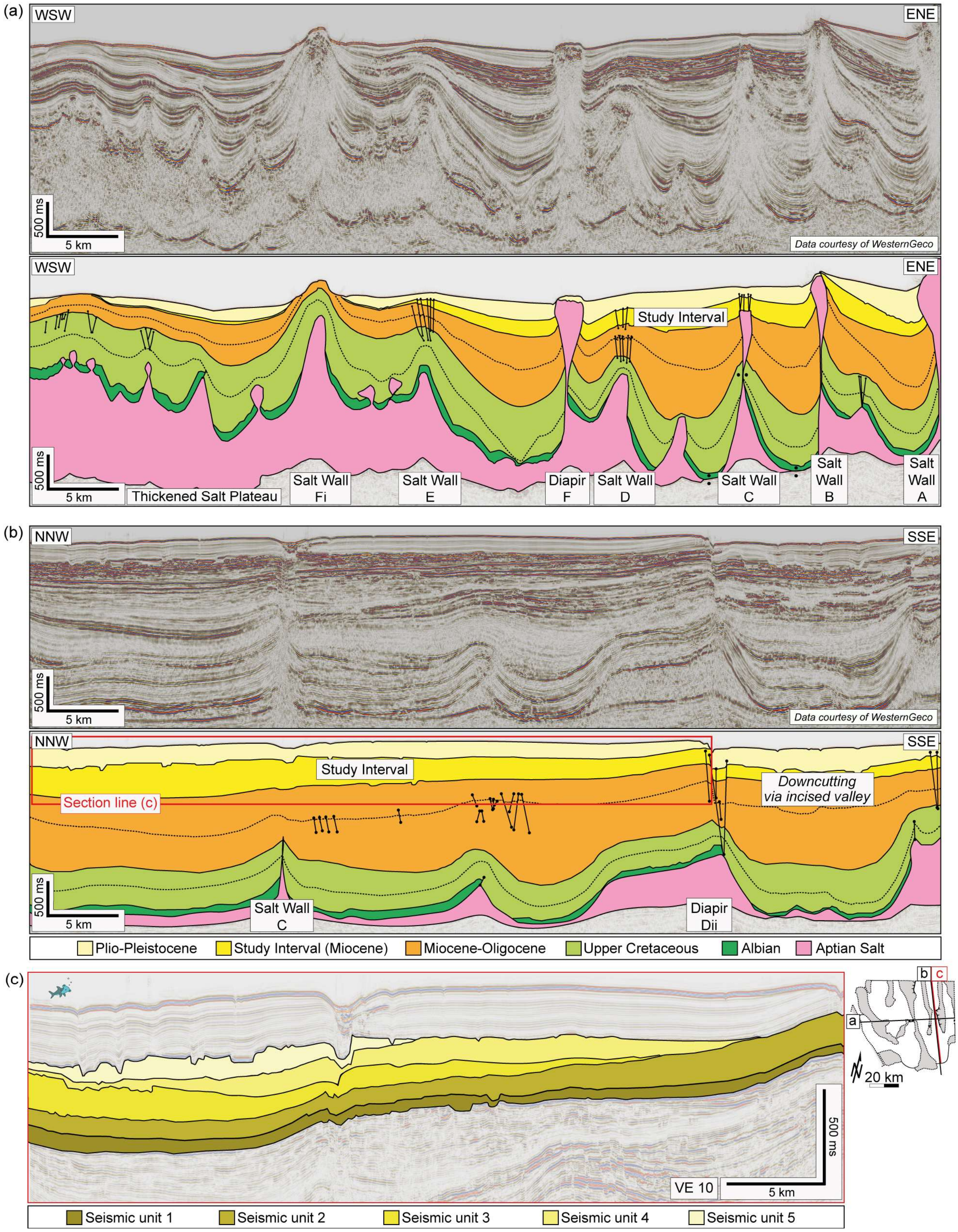

1168

1169 Figure 5

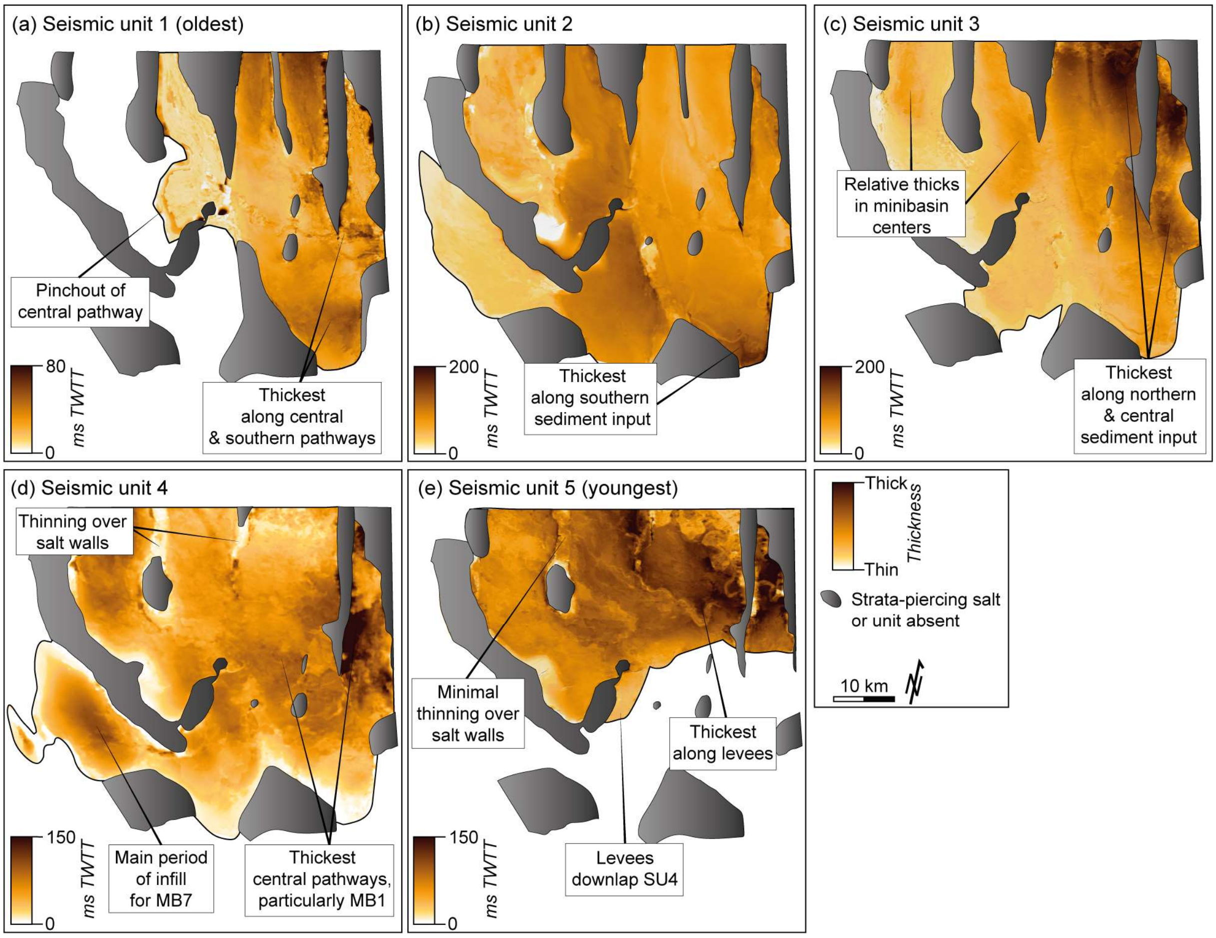

1170

Figure 6

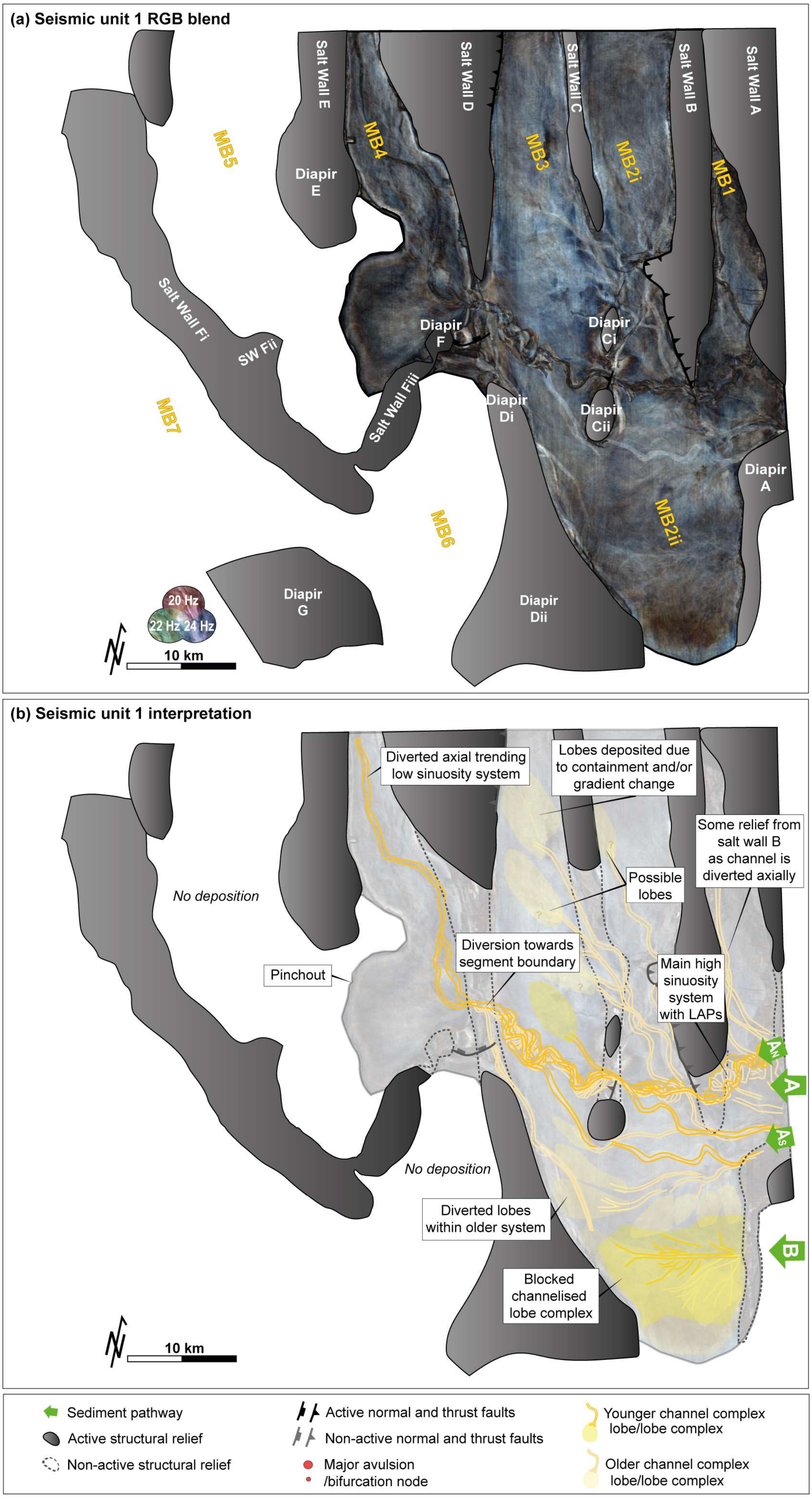

1171

Figure 7

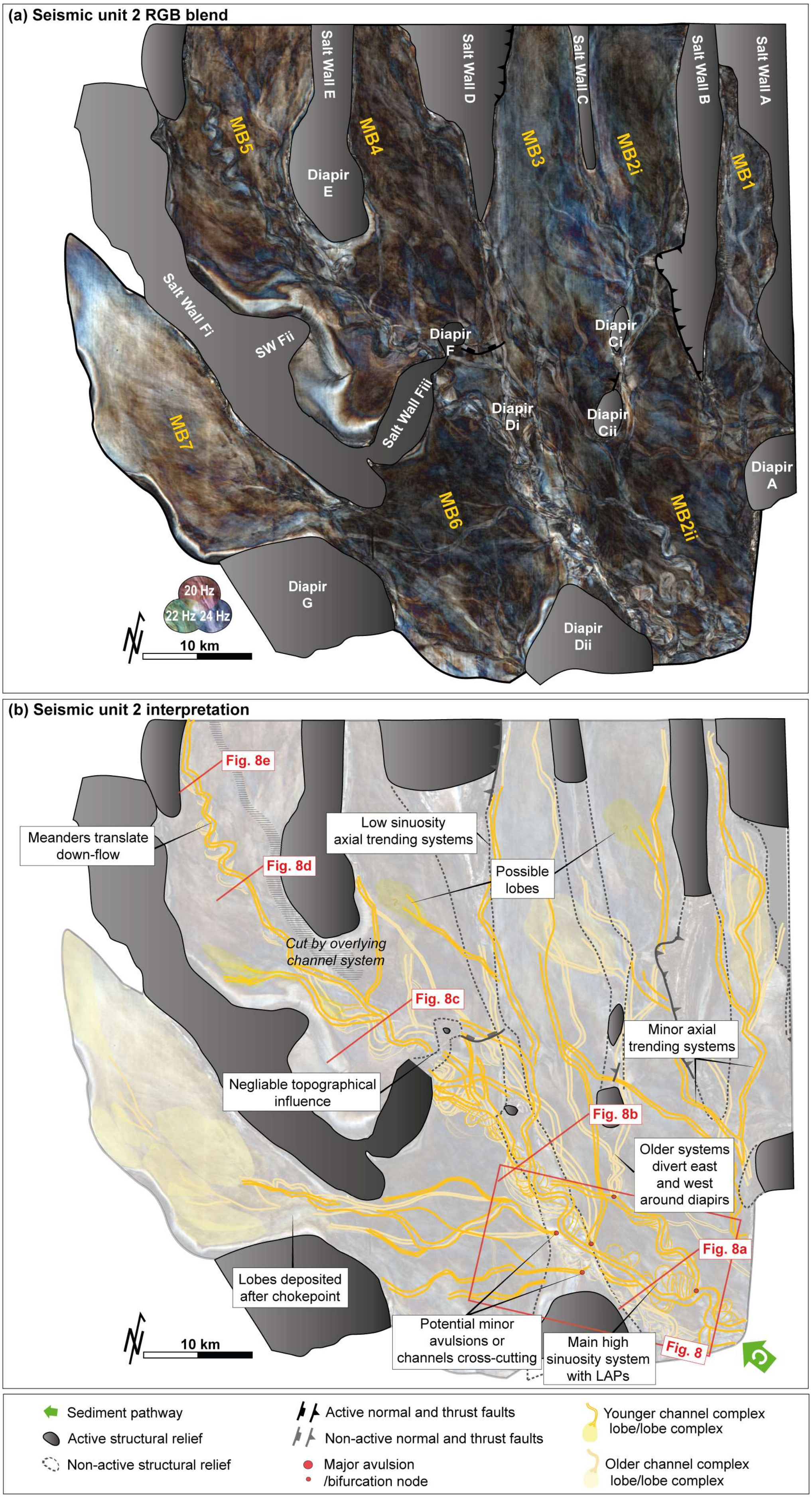

1172

1173 Figure 8

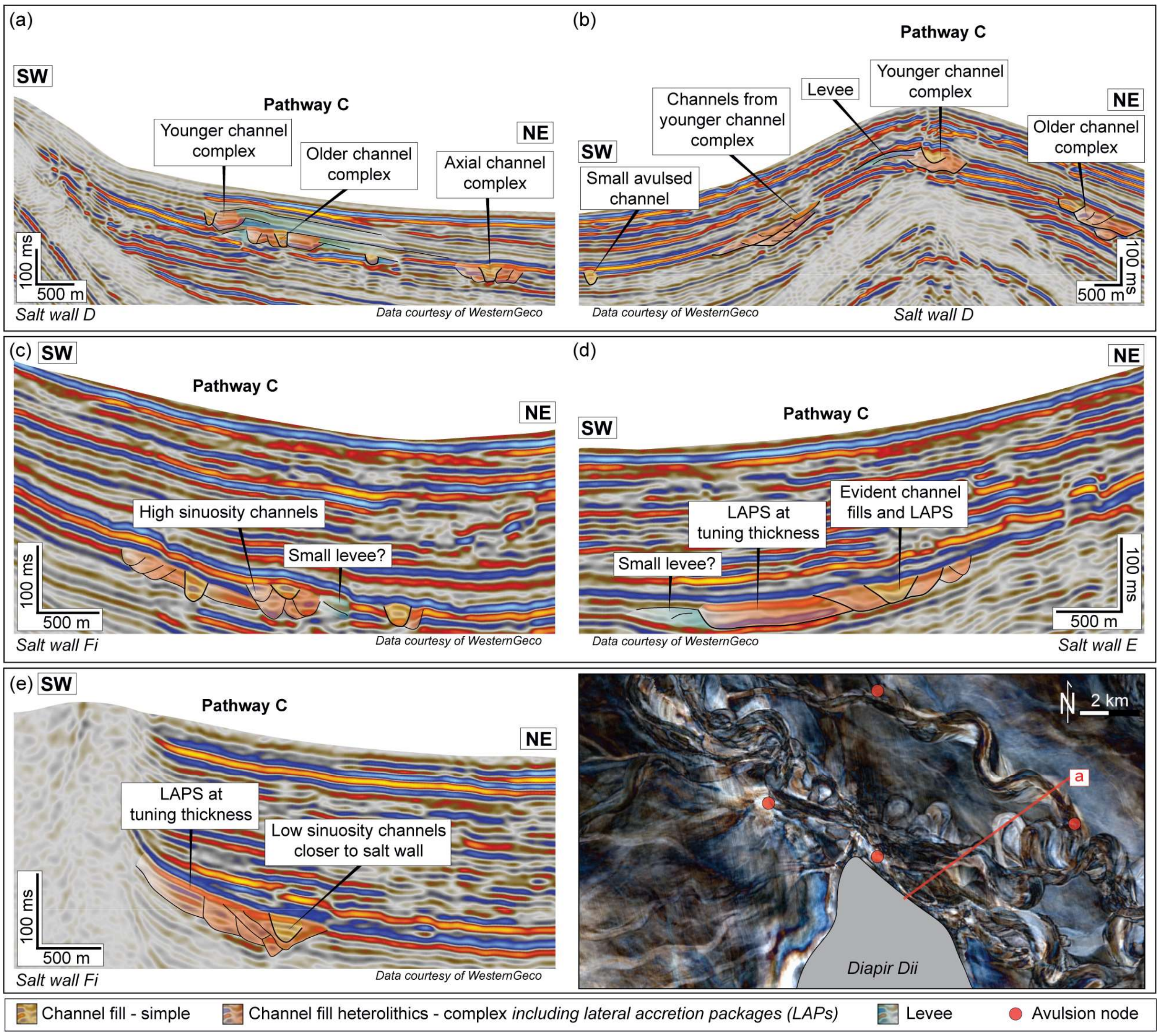

1174

Figure 9

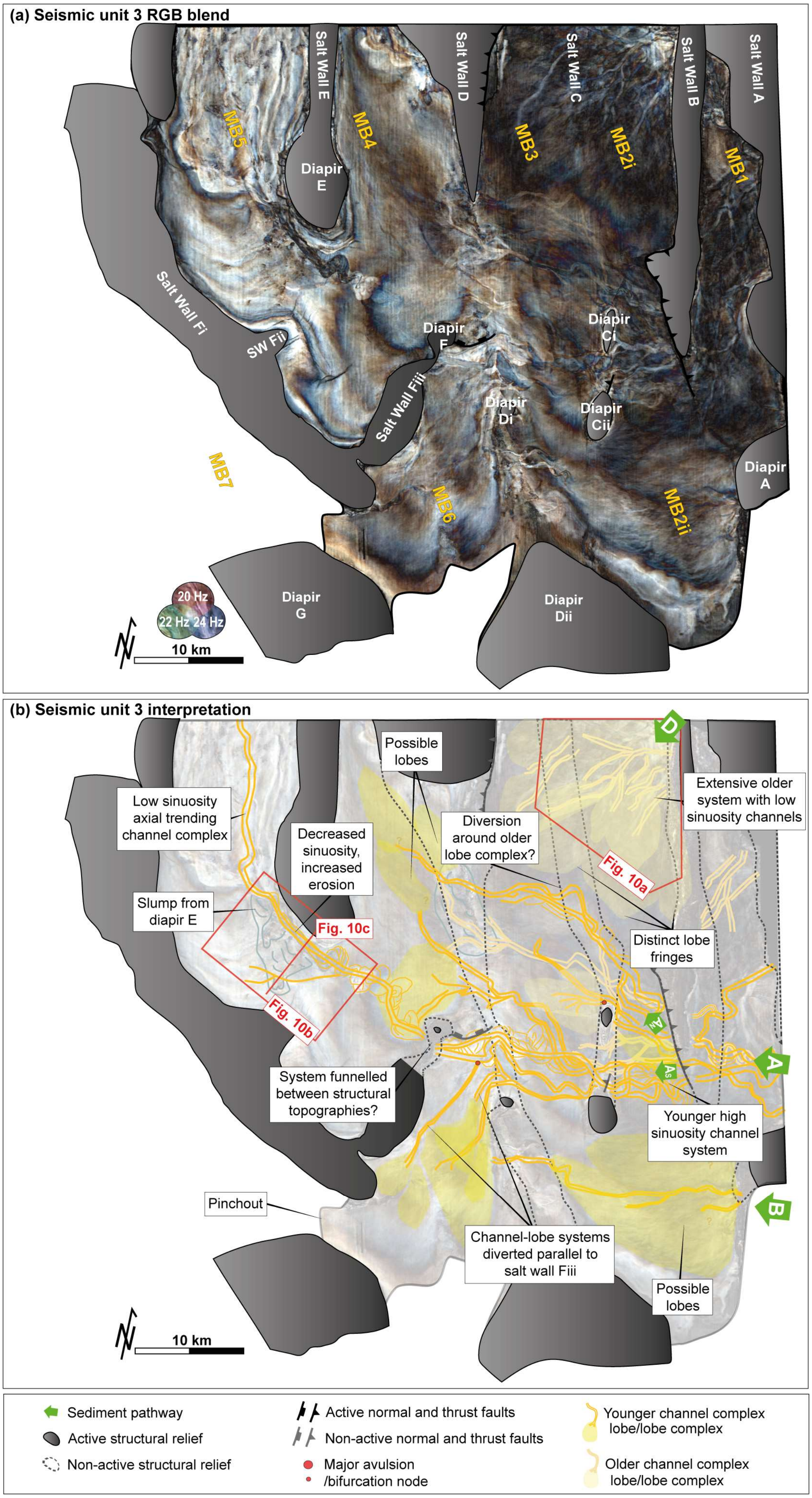

1175

1176 Figure 10

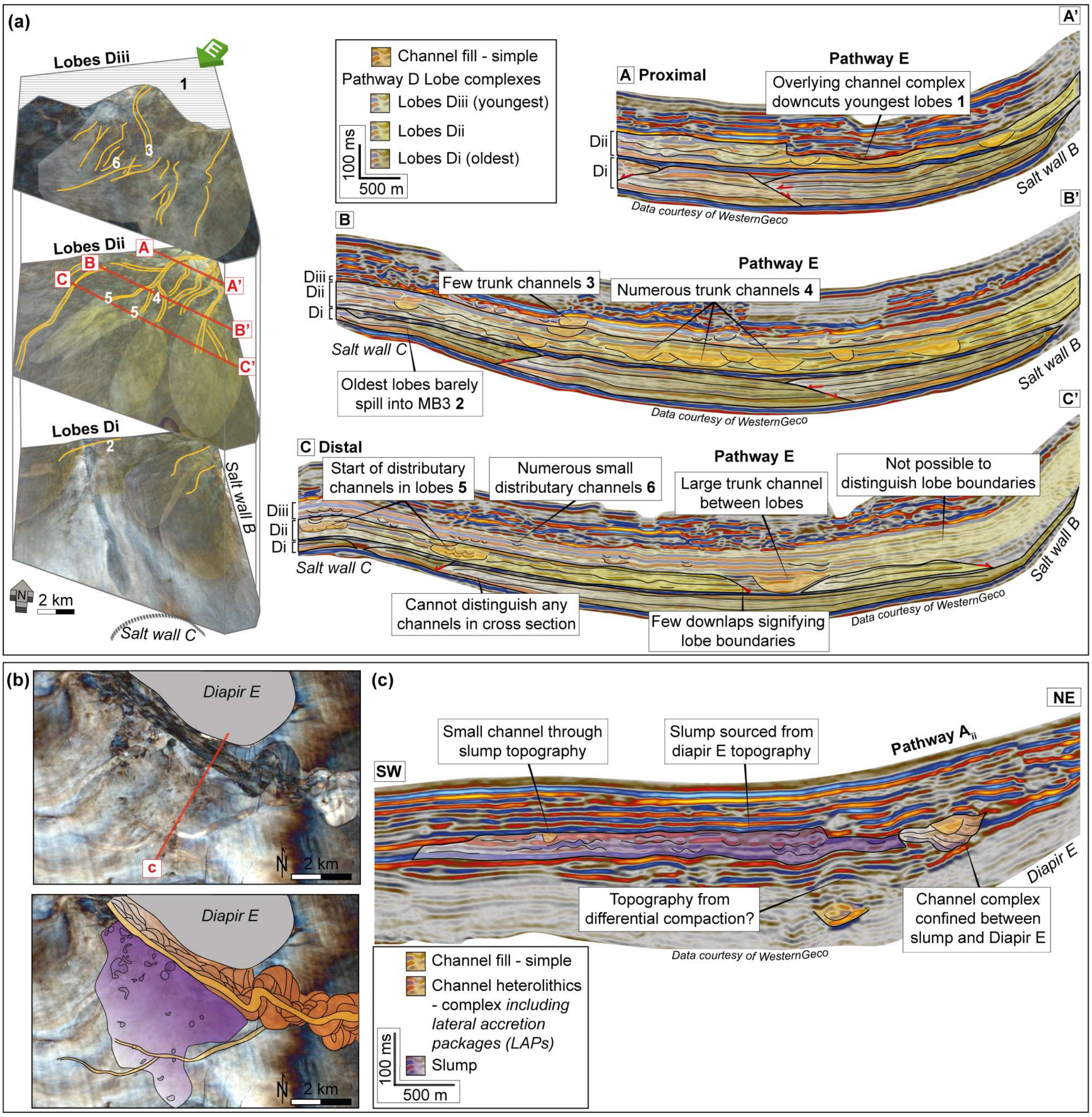

1177

Figure 11

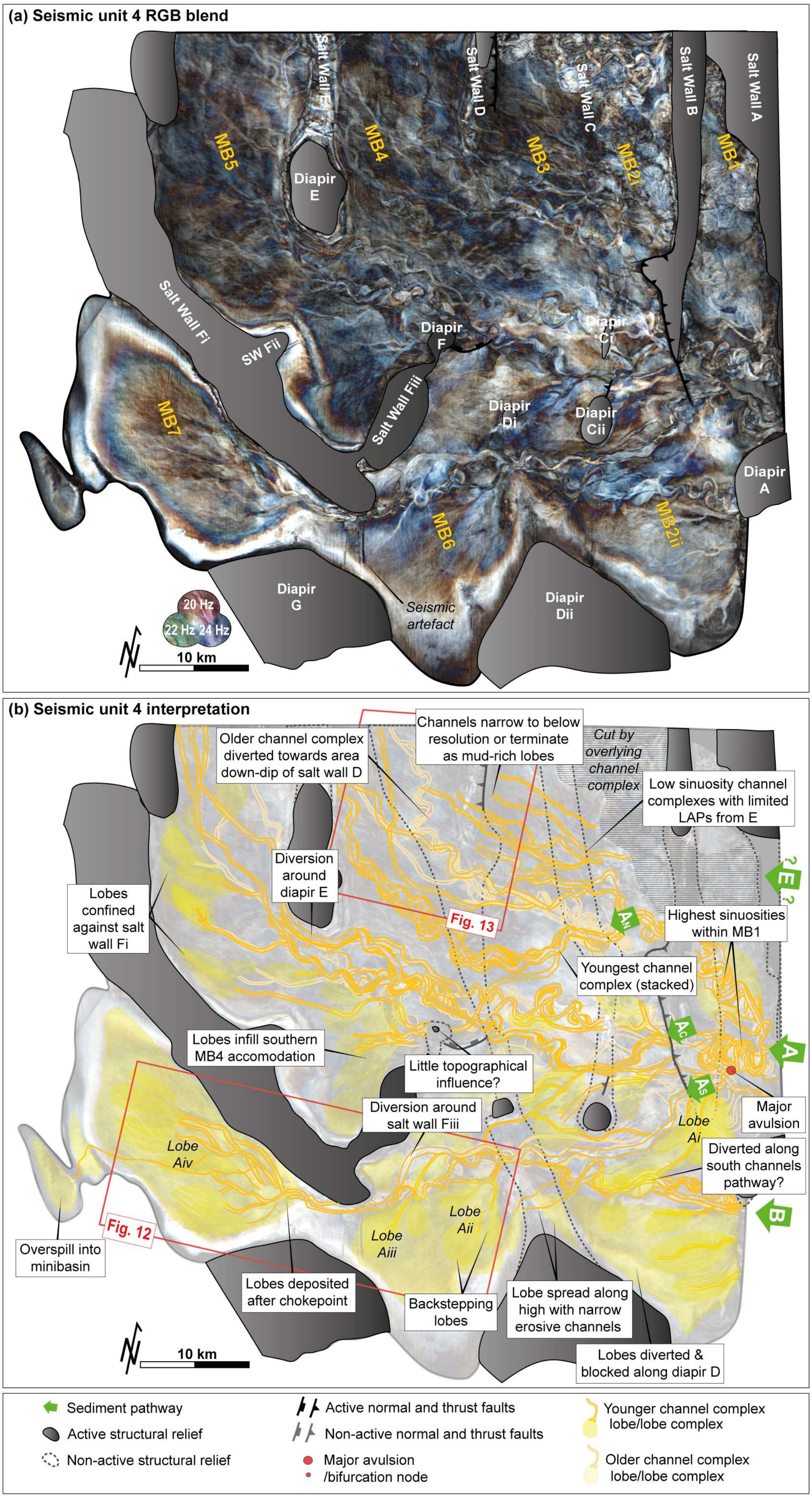

1178

1179 Figure 12

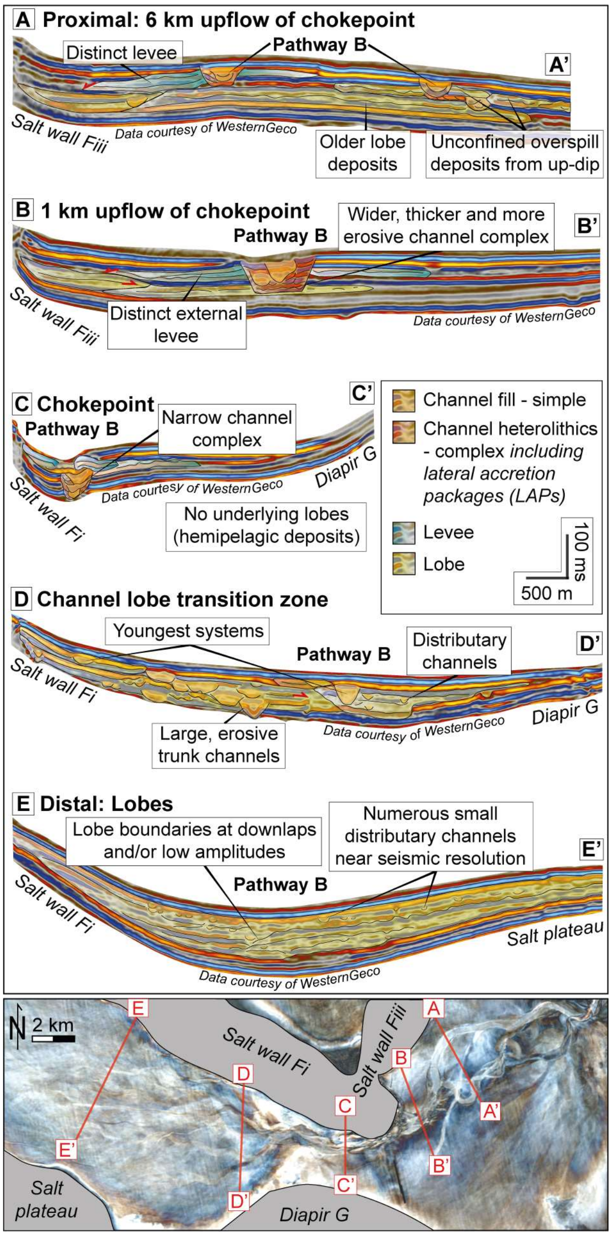

1180

Figure 13

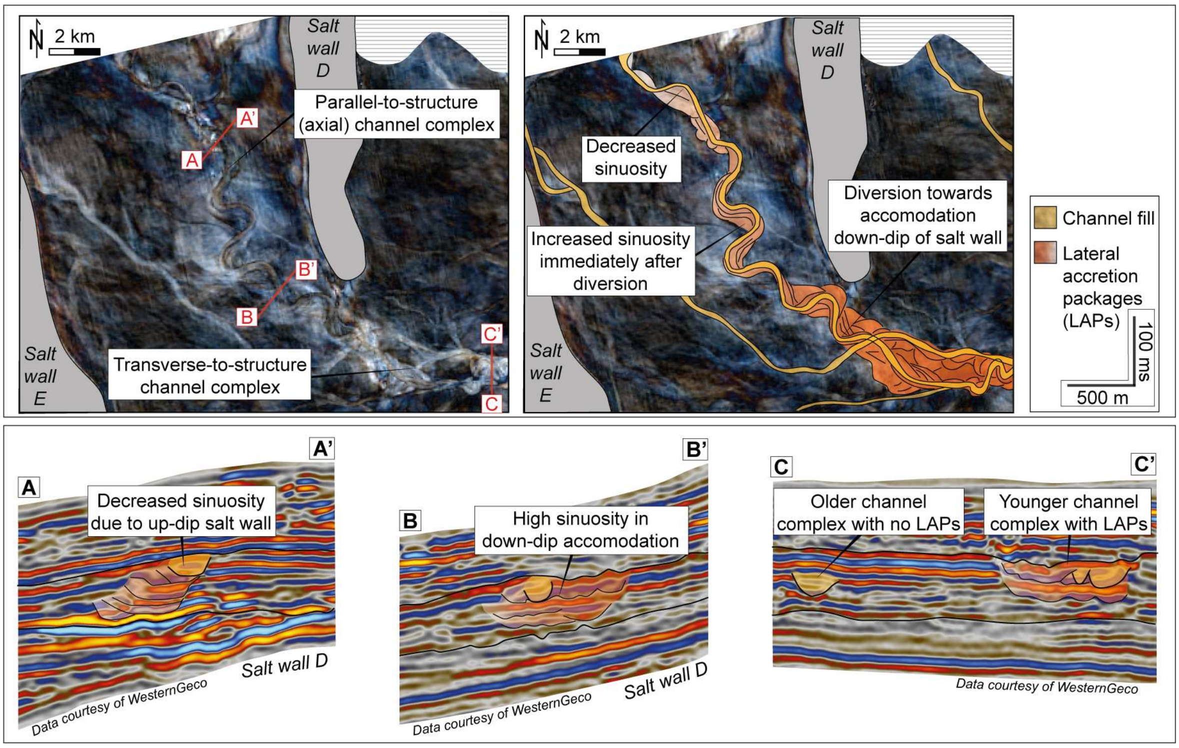

2 km
Salt wall D
Parallel-to-structure (axial) channel complex
A'
A
B'
B
C'
C
Salt wall E
Transverse-to-structure channel complex
Decreased sinuosity
Diversion towards accomodation down-dip of salt wall
Increased sinuosity immediately after diversion
Channel fill
Lateral accretion packages (LAPs)
100 ms
500 m
Decreased sinuosity due to up-dip salt wall
Salt wall D
Data courtesy of WesternGeco
High sinuosity in down-dip accomodation
Older channel complex with no LAPs
Younger channel complex with LAPs

Figure 14

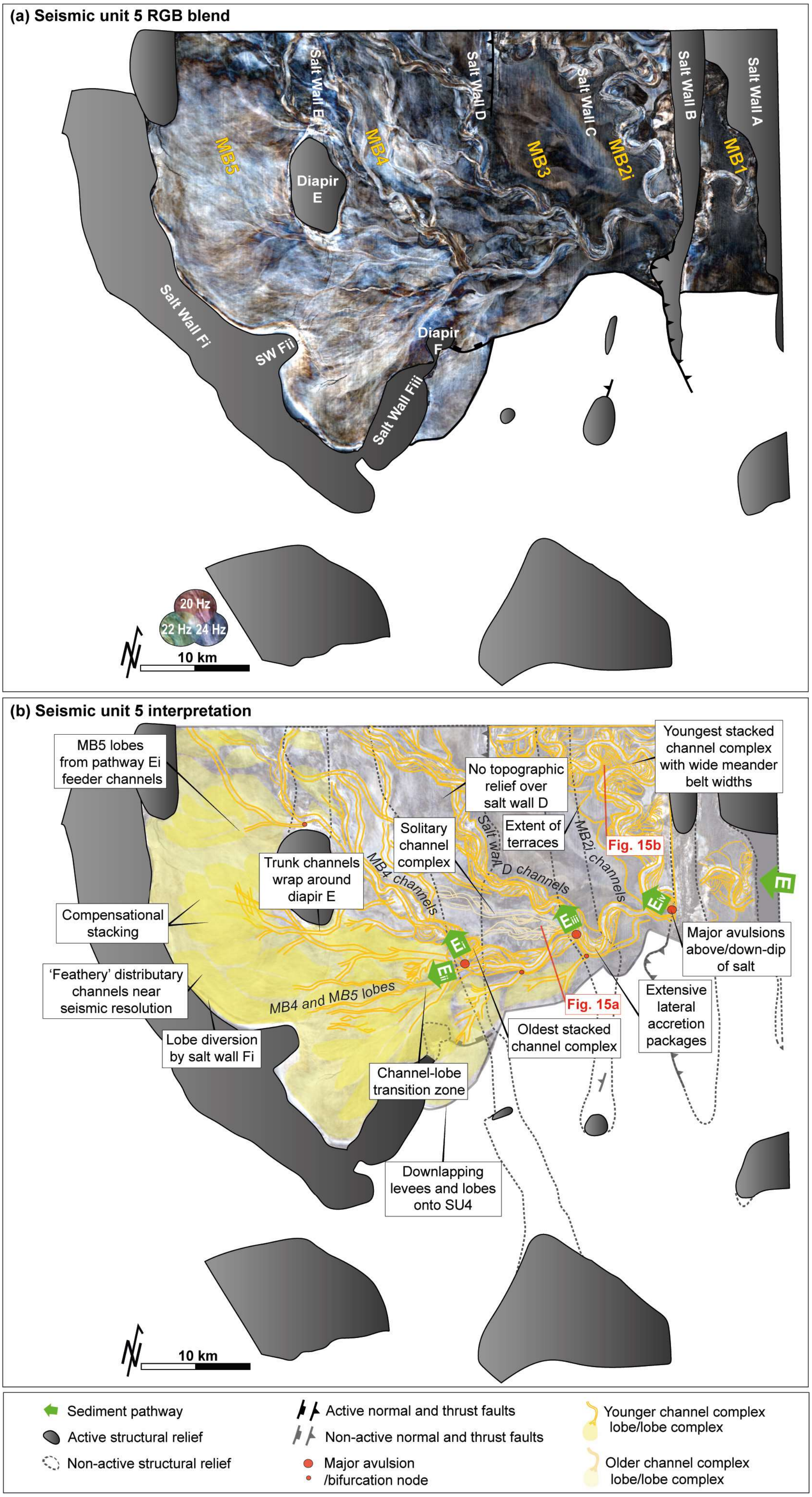

1183

1184 Figure 15

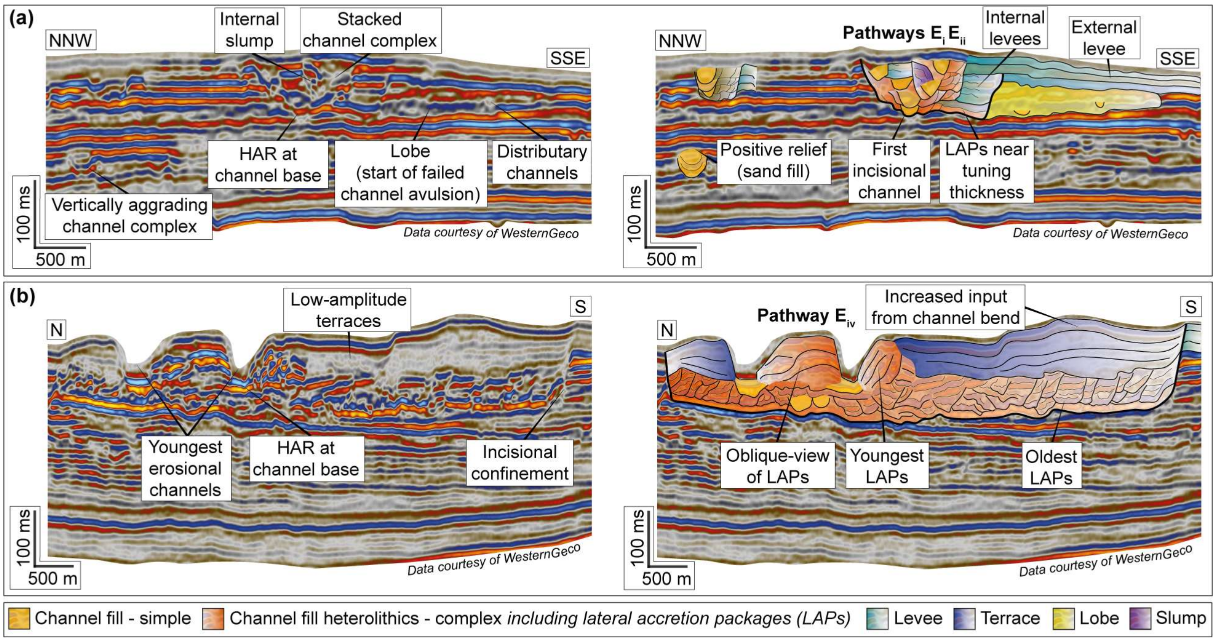

1185

Figure 16

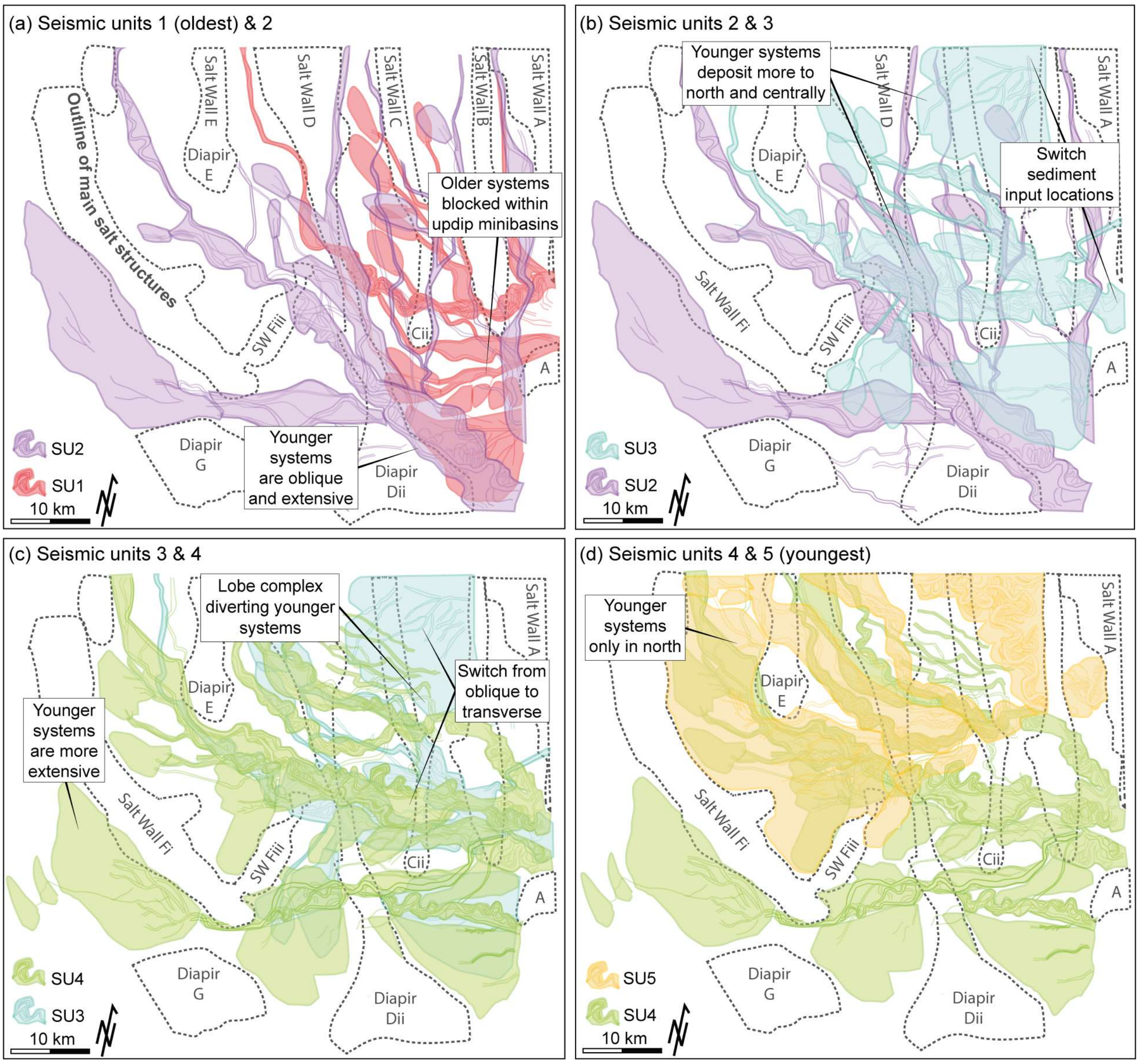

(a) Seismic units 1 (oldest) & 2
Outline of main salt structures
Salt Wall E
Salt Wall D
Salt Wall C
Salt Wall B
Salt Wall A
Diapir E
SW Fiii
Cii
A
Diapir G
Diapir Dii
Older systems blocked within updip minibasins
Younger systems are oblique and extensive
SU2
SU1
10 km
(b) Seismic units 2 & 3
Younger systems deposit more to north and centrally
Switch sediment input locations
Salt Wall D
Salt Wall A
Diapir E
Salt Wall Fi
SW Fiii
Cii
A
Diapir G
Diapir Dii
SU3
SU2
10 km
(c) Seismic units 3 & 4
Lobe complex diverting younger systems
Switch from oblique to transverse
Younger systems are more extensive
Salt Wall A
Diapir E
Salt Wall Fi
SW Fiii
Cii
A
Diapir G
Diapir Dii
SU4
SU3
10 km
(d) Seismic units 4 & 5 (youngest)
Younger systems only in north
Salt Wall A
Diapir E
Salt Wall Fi
SW Fiii
Cii
A
Diapir G
Diapir Dii
SU5
SU4
10 km

1188 Figure 17

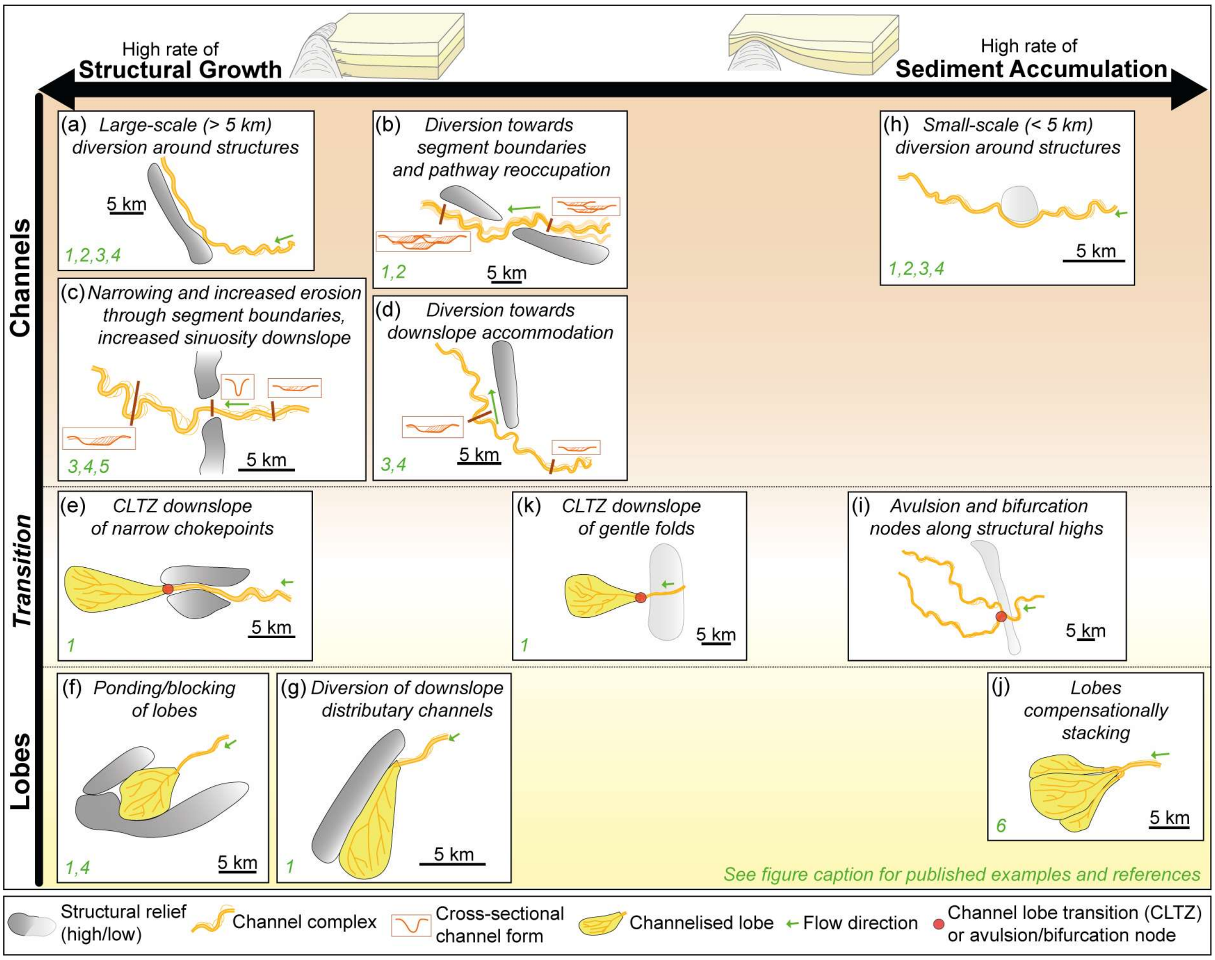

1189

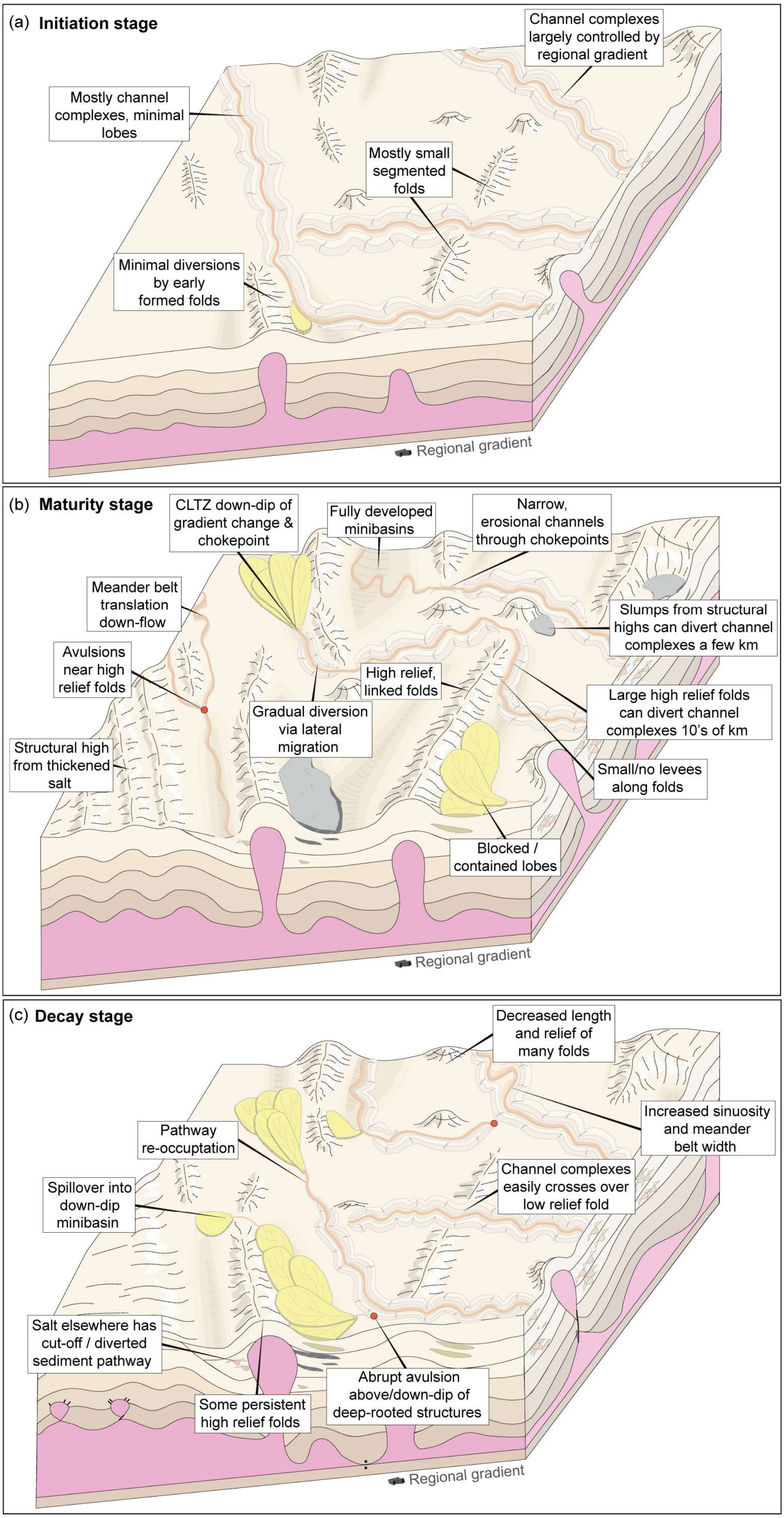
(a) Initiation stage
Channel complexes largely controlled by regional gradient
Mostly channel complexes, minimal lobes
Mostly small segmented folds
Minimal diversions by early formed folds
Regional gradient
(b) Maturity stage
CLTZ down-dip of gradient change & chokepoint
Fully developed minibasins
Narrow, erosional channels through chokepoints
Meander belt translation down-flow
Slumps from structural highs can divert channel complexes a few km
Avulsions near high relief folds
High relief, linked folds
Gradual diversion via lateral migration
Large high relief folds can divert channel complexes 10's of km
Structural high from thickened salt
Small/no levees along folds
Blocked / contained lobes
Regional gradient
(c) Decay stage
Decreased length and relief of many folds
Increased sinuosity and meander belt width
Pathway re-occuptation
Channel complexes easily crosses over low relief fold
Spillover into down-dip minibasin
Salt elsewhere has cut-off / diverted sediment pathway
Some persistent high relief folds
Abrupt avulsion above/down-dip of deep-rooted structures
Regional gradient

1190

Table 1

	Seismic Unit (SU)	Bounding Horizons	Horizon Characteristics	Reflector Geometries
		F	Series of downlapping high amplitude peaks separating from above low amplitude Plio-Pleistocene above	
Youngest	SU5			Continuous high amplitude reflectors across northern minibasins, conformable with underlying salt-cored highs. Downlaps onto SU4
		E	Regionally continuous high amplitude trough. Not a major bounding horizon but marks a gradual facies transition from underlying unit	
	SU4			Continuous low and medium amplitude reflectors with limited onlapping to underlying salt-cored highs. Eroded by SU5 in parts of MB1, MB2i. Onlaps onto SU2
		D	Regionally continuous distinct high-amplitude peak separating from dipping reflectors in the unit below	
	SU3			Largely low amplitude reflectors, downlaps onto SU2
		C	Regionally continuous distinct high-amplitude peak (-trough set) with downlapping reflectors in north	
	SU2			Continuous medium amplitude conformable (to horizon B) reflectors
		B	Distinct high-amplitude trough (-peak set). Does not continue across all minibasins	
Oldest	SU1			Continuous low amplitude conformable (to horizon A) reflectors onlapping major salt walls / confined to up-dip minibasins
		A	Distinct high-amplitude trough (-peak set) separating from lower-amplitude reflectors below. Does not continue across all minibasins	

Table 2

Seismic facies Reflection character	Reflection geometry	Depositional environment	Seismic cross-section	RGB blend map
Submarine channels ***Channel fill – simple*** Semi-parallel low or high amplitude reflections	V-shaped channel form with distinct basal surface. Top surface varies from horizontal to convex-up. Up to c. 50 ms TWTT, width c. 0.25 km, > 50 km length	Erosionally confined stacked channel belts with alternating dominating lithologies, sand or mud fill	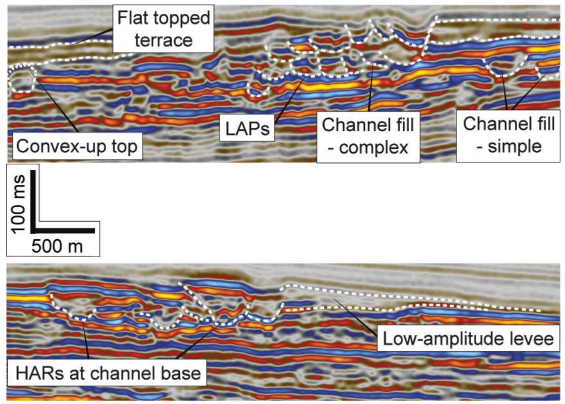	
Channel fill – complex High amplitude reflections (HARs) at base, often overlain by discontinuous variable amplitude reflections	U-shaped channel form, shingled reflections often overlain by parallel reflections. Up to c. 100 ms TWTT, width c. 1 km, > 50 km length	Sinuous meandering and levee-confined stacked channel belts with variable composition; includes lateral accretion packages (LAPs) from channel migration		
Levees Variable (low to high) amplitude, sub-parallel and semi-continuous reflections	Gull wing to wedge shaped taper forms, thinning away from channel fills Up to 80 ms TWTT thick, max. c. 12 km wide	Overbank deposits from turbidity currents within channels, often fine-grained but can be sand-rich; includes flat-topped terraces		
Lobes High (to medium) amplitude reflection packages (HARPs), sub-parallel and semi-continuous (< 15 km)	Tabular to mounded morphology, downlaps or amplitude change near edges Up to c. 100 ms TWTT thick (complex), c. 1 km by 5 km (lobes) up to c. 8 km to c. 20 km (complex) lateral extents	Deposits of unconfined flows at channel mouths, mostly sand-rich; includes channelised terminal lobes and unchannelised crevasse splays	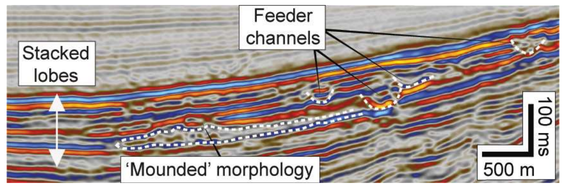	
Slumps Variable (low to moderate) amplitude, discontinuous to chaotic reflections	Erosive basal surface, undular top surface, some internal thrusts and mounds Up to c. 50 ms TWTT thick, c. 15 km lateral extent	Deposits of gravity driven mass wasting from topographic highs, variable composition	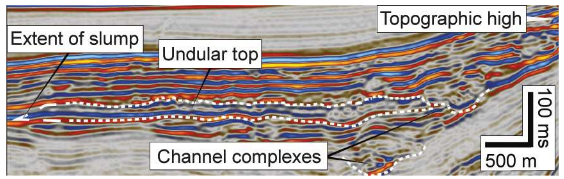	
Slope deposit Variable (low to moderate), parallel and continuous reflections	Continuous and parallel (concordant with below deposits), minor normal faulting Up to 100's of ms TWTT thick, 10's of km laterally	Background fine-grained sedimentation in low energy environments or mud-rich turbidity currents